Remote Sensing of Environment 186 (2016) 596–615

Contents lists available at ScienceDirect

Remote Sensing of Environment

journal homepage: www.elsevier.com/locate/rse

Fluspect-B: A model for leaf fluorescence, reflectance and transmittance spectra

Nastassia Vilfan[a,*], Christiaan van der Tol[a], Onno Muller[b], Uwe Rascher[b], Wouter Verhoef[a]

[a] University of Twente, Faculty of Geo-Information Science and Earth Observation (ITC), P.O. Box 217, AE Enschede 7500, The Netherlands
[b] Institute for Bio- and Geosciences, IBG-2: Plant Sciences, Forschungszentrum Jülich GmbH, Jülich 52425, Germany

ARTICLE INFO

Article history:
Received 4 February 2016
Received in revised form 23 August 2016
Accepted 14 September 2016
Available online xxxx

JEL classification:
2010 MSC: 00-01
99-00

Keywords:
Leaf chlorophyll fluorescence
Reflectance
Transmittance
Radiative transfer model
Leaf optical properties

ABSTRACT

We present the Fluspect-B model (generally referred to as Fluspect), which simulates leaf chlorophyll fluorescence (ChlF), reflectance and transmittance spectra. The existing PROSPECT model and its concept of a compact leaf are used as a starting point, and the differential equations for radiative transfer within the leaf are solved by an efficient doubling algorithm. Due to the simplicity of these equations, Fluspect offers a high computational speed. With incident light provided as the main input parameter, Fluspect calculates the emission of ChlF on both the illuminated and shaded side of the leaf. Other input parameters are chlorophyll and carotenoid concentrations, leaf water, dry matter and senescent material (brown pigments) content, leaf mesophyll structure parameter and ChlF quantum efficiency for the two photosystems, PS-I and PS-II. We investigated the model performance using measurements of leaf reflectance, transmittance and ChlF spectra, collected for barley and sugar beet leaves in both a laboratory and outdoors setting. The plants had been grown under various illumination conditions to increase between-leaf variability of leaf biochemical and structural properties. We retrieved the model parameters, compared them to corresponding destructive measurements and finally, used them to simulate ChlF on either side of the leaf at several light intensities. The results show that the model reproduces observed SIF accurately, especially for leaves measured under natural illumination. Most of the observed between-leaf variability of ChlF could be explained from differences in leaf biochemical and structural properties, with potential additional information held by ChlF emission efficiency parameters.

1. Introduction

Spectroscopy has long been used as a non-invasive technique for the detection and analysis of plant physiological and anatomical traits (Buschmann and Nagel, 1993). Several models have been developed in order to non-destructively predict the effects of leaf pigment content and internal structure on both reflectance and transmittance (Ustin et al., 2009). Physically based radiative transfer models have been developed and modified since the early 1990s. A few examples include PROSPECT (Leaf Optical Properties Spectra) developed by Jacquemoud and Baret (1990), LIBERTY (Leaf Incorporating Biochemistry Exhibiting Reflectance and Transmittance Yields) (Dawson et al., 1998) and the work of Stuckens et al. (2009).

Besides plant reflectance and transmittance, the emission of plant chlorophyll fluorescence (ChlF) has also been demonstrated to be an important signal. Measurements of solar-induced ChlF (SIF) have introduced a new remote sensing method for tracking photosynthesis and gross primary productivity (GPP) from leaf and canopy to airborne and potentially, satellite scale (Moreno et al., 2014; Porcar-Castell et al., 2014).

ChlF provides information on the dynamic behaviour of photosynthesis (for a review, see Porcar-Castell et al., 2014). The signal originates in the antennae complexes of photosystems I and II (PS-I and PS-II), and a green leaf will emit ChlF upon excitation with photosynthetically active light (wavelengths between 400–700 nm). The ChlF signal is variable and most of its variability at ambient temperatures has been shown to originate in photosystem II (Franck et al., 2002). The efficiency of photosynthesis is regulated and responds to environmental constraints. As most of the regulation of photosynthesis takes place in PS-II, and because ChlF is mainly emitted from PS-II, the ChlF signal is a good indicator of the functional status of photosynthesis and is related to the light use efficiency (LUE) of photosynthesis (Ač et al., 2015; Hilker et al., 2008).

Tracking the variability of ChlF over time offers a direct non-destructive approach to detecting plant stress before the stress results in any significant reduction in chlorophyll content,

* Corresponding author.
E-mail address: n.rajhvilfan@utwente.nl (N. Vilfan).

http://dx.doi.org/10.1016/j.rse.2016.09.017
0034-4257/

both at the leaf and more remote scales (Campbell et al., 2008; Frankenberg et al., 2011; Joiner et al., 2011; Meroni et al., 2009; Rossini et al., 2015; Van Wittenberghe et al., 2013). The ChlF signal has been used to study, for example, seasonal variations (Guanter et al., 2012; Joiner et al., 2011), the effects of pollutants (Eullaffroy and Vernet, 2003; Van Wittenberghe et al., 2013), water stress (Dobrowski et al., 2005; Panigada et al., 2014) and nitrogen deficiencies (Campbell et al., 2008; Tremblay et al., 2011).

As with reflectance and transmittance, ChlF depends on leaf pigment content (predominantly chlorophyll concentration, but other constituents as well) and anatomy. Over the short term (seconds to a few days), we can assume that leaf biochemical and structural properties do not change. However, rapid variations in ChlF emission are still observed in response to changes in incoming light and various stress factors (Ač et al., 2015). These rapid variations in ChlF are due to variations in the fluorescence quantum efficiency (η); where η is expressed as a fraction of the radiation absorbed by the chlorophyll. This efficiency is inversely proportional to the photochemical (PQ) and non-photochemical quenching (NPQ), derived from measurements of active ChlF (Demmig et al., 1987; Krause and Weis, 1984). Variations in the efficiency are usually measured by taking repeated measurements of ChlF on the same leaf, while exposing the leaf to varying light conditions, CO_2 concentrations, air temperatures and humidities (Genty et al., 1989; Weis and Berry, 1987).

When measuring the solar-induced ChlF (SIF) of natural vegetation canopies in uncontrolled conditions over longer time scales (several days to seasons), then leaf biochemistry, structure and η vary together in space and time (Cogliati et al., 2015). It is then more difficult to retrieve η, leaf biochemical and structural properties separately (Porcar-Castell et al., 2014).

In several recent publications (Lee et al., 2015, 2013; Zhang et al., 2014), the SCOPE model (Van der Tol et al., 2009) has been used for this purpose. SCOPE simulates radiative transfer in the leaf and canopy; and variations in the quantum efficiency as affected by various stress factors. SCOPE consists of several routines that are separate models: some nested and some executed in cascade. In such a model, equifinality can be a real problem. Therefore is it useful to evaluate its components separately using controlled experiments. A model component that simulates leaf ChlF based on a conventional photosynthesis model has been reported (Van der Tol et al., 2014), but a separate evaluation of the leaf level radiative transfer component of the model, named Fluspect, has not been published previously. An early version was presented in a conference paper (Verhoef, 2011), but since then, the model has undergone several revisions.

Fluspect is a radiative transfer model that simulates the leaf reflectance, transmittance and ChlF for a given emission efficiency and a given spectral shape of ChlF for PS-I and PS-II emission (Miller et al., 2005). It is similar but computationally simpler, and consequently faster, than the FluorMODleaf model (Pedrós et al., 2010), which is to our knowledge the only leaf radiative transfer model for ChlF reported in the literature to date.

The objective of this paper is to present and evaluate the Fluspect model. We first describe the latest version of the model, namely Fluspect-B (Section 2 and the Appendices). This is followed by a description of an experiment in which data were collected for model performance evaluation (Section 3.1). The model evaluation is achieved by first retrieving the leaf biochemical and structural (PROSPECT) parameters from measured reflectance and transmittance by means of model inversion (Section 3.2), and consequently using the retrieved parameters to simulate ChlF (Section 3.3). In the Results and discussion section, we compare the simulated to measured reflectance and transmittance (Section 4.1), the retrieved to measured parameters (Section 4.2), and the simulated to measured ChlF (Section 4.3). In Section 4.4 we show the results of a sensitivity analysis of the model. Conclusions are presented in Section 5.

2. Model description

Here we present the latest version, called Fluspect-B, implemented in Matlab and published under GNU General Public License at https://github.com/christiaanvandertol. Fluspect-B parameters, together with their range and standard values, are defined in Table 1.

The model takes the PROSPECT model (Jacquemoud et al., 2009) as its starting point to compute the two fluorescence matrices g (backward direction, that is ChlF detected from the leaf side turned toward the light source, and in this study we exclusively illuminated the adaxial leaf side) and f (forward direction, i.e. ChlF detected from the leaf side turned away from the light source; in this study, the abaxial leaf side) by means of a fast doubling method. During this doubling process also leaf reflectance and transmittance are reproduced. This was done by applying the Kubelka-Munk (KM) theory of diffuse scattering and absorption to the whole leaf (Kubelka and Munk, 1931). The starting doubling equations are just an expression of the KM differential equations with fluorescence effects added. After 15 doubling steps the reflectance and transmittance spectra are obtained, which are identical to those of PROSPECT, while the fluorescence matrices are obtained as useful by-products.

In Fluspect-B, the doubling algorithm that generates the fluorescence matrices of the leaf is no longer applied to the complete leaf as computed with PROSPECT, but only to the leaf mesophyll layer, which is obtained after "removing" the top and bottom leaf-air interfaces. The reflectance and transmittance (ρ and τ) of this mesophyll layer are now taken as the starting point to calculate the KM scattering and absorption coefficients, and these are applied along with the fluorescence spectra of photosystems I and II as a basis for the doubling algorithm. The outcomes of the doubling algorithm are reflectance and transmittance ρ and τ, plus the fluorescence matrices g and f, for the backward and forward fluorescence of the leaf mesophyll layer, respectively. In the last step, these internal leaf fluorescence matrices are modified to include again the effects of the leaf-air interfaces.

In the first version of Fluspect (Verhoef, 2011), the model showed discrepancies with FluorMODleaf (Pedrós et al., 2010), especially when fluorescence was plotted as a function of the chlorophyll content, but this problem has been resolved as follows.

2.1. PROSPECT background

The model PROSPECT is based on the concept of a so-called compact leaf and it uses the so-called plate theory (Allen et al., 1969) to describe radiative transfer at the surface and inside plant leaves. Only diffuse fluxes in backward and forward direction are considered in this theory.

Throughout the paper, the flux interactions are illustrated with boxes and circles, where a square box stands for incident radiation and a circle for reflected or transmitted radiation. The boxes and circles are connected by arrows that indicate the direction of flow, and a symbol next to the arrow indicates the corresponding reflectance or transmittance. Forward fluxes are placed on the left and backward fluxes on the right. Since reflection always takes place at the same vertical level (that is, for a horizontal plate), and transmission goes from a certain level to one level lower or higher, reflections are indicated by horizontal arrows and transmissions by vertical arrows. Circles and boxes connected by solid bars refer to one and the same vertical level.

Fig. 1 illustrates the interactions between the fluxes if a single layer is illuminated by forward flux at the top and backward flux at the bottom. There are two reflectances, one at the top (R_t) and one at

Table 1
Fluspect input parameters.

Parameter	Symbol	Range	Standard value	Unit	Reference	Origin
Chlorophyll a+b content	C_{ab}	0–100	40	µg cm^{-2}	Jacquemoud and Baret (1990)	PROSPECT
Total carotenoid content	C_{car}	0–30	5	µg cm^{-2}	Feret et al. (2008)	PROSPECT
Water content	C_w	0–0.4	0.009	cm	Jacquemoud and Baret (1990)	PROSPECT
Dry matter content	C_{dm}	0–0.5	0.012	g cm^{-2}	Jacquemoud and Baret (1990)	PROSPECT
Leaf mesophyll structure parameter	N	1–4	1.5	–	Jacquemoud and Baret (1990)	PROSPECT
Senescence material (brown pigments)	C_s	0–0.6	0	fraction	Jacquemoud and Baret (1990)	PROSPECT
Fluorescence quantum efficiency for PS-I	η_I	0–0.2	0.002	–	Miller et al. (2005)	Fluspect
Fluorescence quantum efficiency for PS-II	η_{II}	0–0.2	0.01	–	Miller et al. (2005)	Fluspect

the bottom (R_b), and two transmittances, one forward (T_d) and one backward (T_u).

The interface between two media of different refraction index has no thickness, but will yet be considered as a layer too. A diffusing layer may be bounded by two interfaces to the surrounding air, one at the top and one at the bottom, so that optically it will be described by three layers in total. An example of this is given in Fig. 2a, which illustrates a diffusing layer bounded by two leaf-air interfaces, and where each optical layer is described by two reflectances (one at the top and one at the bottom) and two transmittances (backward and forward). The vertical levels are simply indicated here by the numbers 0, 1, 2, and 3. The forward and backward fluxes are indicated by E^- and E^+, respectively.

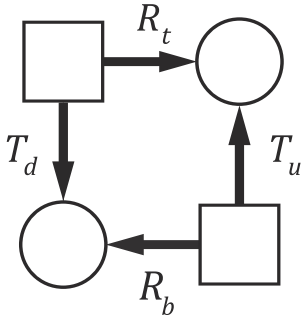

Fig. 1. Two incident fluxes (boxes) producing reflected and transmitted fluxes (circles). The boxes and circles are connected by arrows that indicate the direction of flow, and a symbol next to the arrow indicates the corresponding reflectance or transmittance.

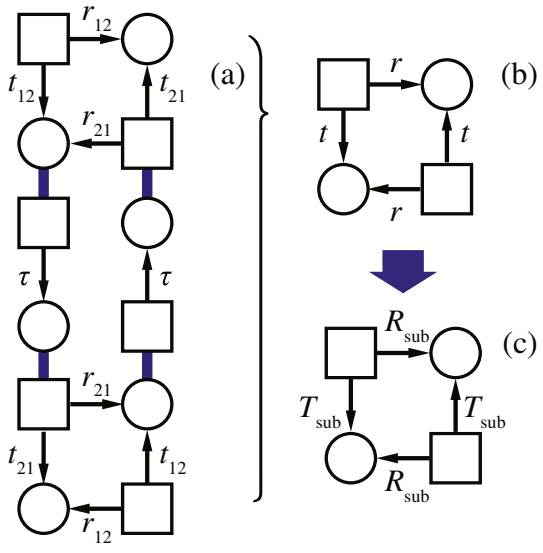

Fig. 2. Flux interaction diagram for (a) a compact leaf as defined in PROSPECT, simplified into (b) a single additional sub-layer and defined as (c) $N-1$ sub-layers (Stokes equations). The boxes and circles are connected by arrows that indicate the direction of flow, and a symbol next to the arrow indicates the corresponding reflectance or transmittance. Circles and boxes connected by solid bars refer to one and the same vertical level.

A compact leaf is a leaf that has two leaf-air interfaces, but the internal leaf mesophyll layer consists only of absorbing materials (as presented in Fig. 2a), namely chlorophylls, carotenoids, water, dry matter and brown pigments, so that scattering and therefore also reflectance are absent. Note that the obtained R and T are dependant on assumed optical properties of these absorbing materials, used in the model as optical parameters.

However, applying PROSPECT to simulate leaves with varying optical properties has led to the conclusion that the compact leaf is not sufficient to capture all spectral variability. Therefore, the non-compact leaf is applied (Allen et al., 1970; Gausman et al., 1970), which consists of a pile of more than one layer (namely N) of compact leaves, where N can also be non-integer. In the latter case, the Stokes equations are used to derive the reflectance and transmittance of a sub layer of $(N)-1$ leaves thick (Fig. 2c). The N parameter in PROSPECT is very important since it can capture the variability of leaf optical properties due to differences in leaf internal scattering and leaf thickness. Finally, the PROSPECT result is obtained by combining the compact top layer with the $(N)-1$ compact layers underneath, giving the final total reflectance R_t and total transmittance T_t, as illustrated in Fig. 2.

The subscripts of the corresponding reflectance (R) or transmittance (T) indicate either the cone incident angle (α), a sub layer ($_{sub}$) or the order of the involved media, for instance, the subscripts "12" indicate that the respective reflectance or transmittance corresponds with a transition of the light from medium 1 (air) to medium 2 (leaf). In the PROSPECT model use is made of the function "tav", which stands for "transmittance average", and which can be calculated for any given cone incidence angle α. This function calculates the transmittance of a non-absorbing rough surface. Traditionally (and also in Fluspect) one takes $\alpha = 59^\circ$ (40° in PROSPECT-5; Feret et al., 2008) for the light incident on the leaf from the outside, whereas for the internal diffuse light one takes $\alpha = 90^\circ$. We acknowledge, that this is a fundamental simplification, as the real BRDF characteristics of leaves are complex and greatly influence leaf reflectance (Jacquemoud and Ustin, 2001).

2.2. Mesophyll reflectance and transmittance

The first step in the whole procedure is the calculation of mesophyll layer reflectance and transmittance, called ρ and τ of the mesophyll layer, from the given PROSPECT leaf reflectance and transmittance (R_t and T_t) and the optical properties of the leaf-air interfaces. Since this element is entirely novel, it is described in some more detail. For this, we use Fig. 3, which illustrates how R_t and T_t are related to ρ and τ.

The effect of the top leaf-air interface is shown in the two rightmost diagrams (Fig. 3b,c), where the reflectance of the background, i.e. the leaf without the leaf-air interface, is indicated by R_b. By

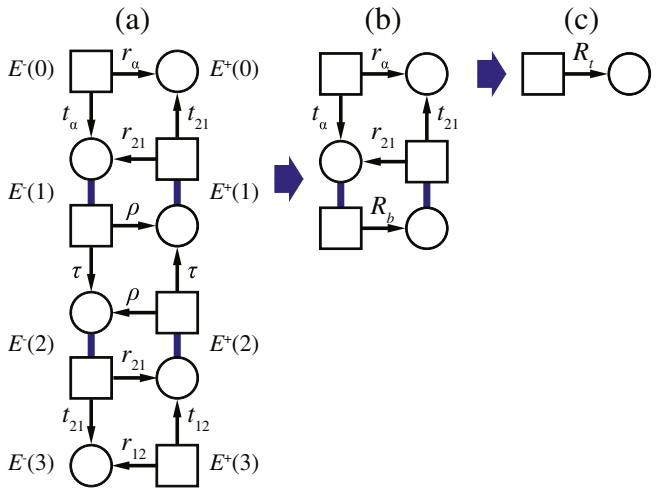

Fig. 3. Flux interaction diagram for (a) a leaf layer with top and bottom border air-leaf interfaces and derived relations between PROSPECT reflectance and transmittance R_t and T_t and reflectance and transmittance of the leaf mesophyll layer, ρ and τ. Diagram (b) depicts the leaf without the leaf-air interface, indicated by R_b and (c) adds the leaf-air interface to this background to obtain the new reflectance R_t. The boxes and circles are connected by arrows that indicate the direction of flow, and a symbol next to the arrow indicates the corresponding reflectance or transmittance. Circles and boxes connected by solid bars refer to one and the same vertical level.

adding the leaf-air interface to this background we obtain the new reflectance R_t, given by

$$R_t = r_\alpha + \frac{t_\alpha R_b t_{21}}{1 - r_{21} R_b} \tag{1}$$

This equation can be easily inverted to obtain R_b from given R_t and some other elementary optical quantities of PROSPECT, which gives

$$R_b = \frac{R_t - r_\alpha}{t_\alpha t_{21} + (R_t - r_\alpha) r_{21}}. \tag{2}$$

The total leaf transmittance T_t of the leaf is found by using Fig. 3 and assuming $E^+(3) = 0$ and $E^-(0) = 1$. This gives

$$E^-(1) = \frac{t_\alpha}{1 - R_b r_{21}}, \qquad E^-(2) = \frac{\tau}{1 - \rho r_{21}} E^-(1), \tag{3}$$

and finally

$$E^-(3) = t_{21} E^-(2). \tag{4}$$

So the total transmittance is the product

$$T_t = \frac{t_\alpha}{1 - R_b r_{21}} \frac{\tau}{1 - r_{21}\rho} t_{21}. \tag{5}$$

Writing

$$Z = \frac{T_t(1 - R_b r_{21})}{t_\alpha} = \frac{\tau}{1 - (r_{21}\rho)}, \tag{6}$$

we obtain a linear equation in ρ and τ which reads

$$(1 - (r_{21}\rho)Z = \tau, \quad \text{or} \quad \tau + r_{21} Z \rho = Z. \tag{7}$$

Note that Z as well as R_b can be obtained from elementary optical quantities in PROSPECT. Since R_b can also be expressed in ρ and τ by

$$R_b = \rho + \frac{\tau^2 r_{21}}{1 - r_{21}\rho} = \rho + \tau r_{21} Z \tag{8}$$

we obtain another linear equation in ρ and τ which reads

$$r_{21} Z \tau + \rho = R_b, \tag{9}$$

so we now have two linear equations in ρ and τ, which can be easily solved to yield

$$\tau = \frac{1 - R_b r_{21}}{1 - (r_{21} Z)^2} Z \quad ; \qquad \rho = \frac{R_b - r_{21} Z^2}{1 - (r_{21} Z)^2}. \tag{10}$$

2.3. Effects of border interfaces on fluorescence

Although the calculation of the border effects on the fluorescence matrices is the last step of the model, it is described here since the same quantities as used in the previous section are used here again. From here onwards, excitation and fluorescence fluxes are symbolized using the letters E and F, respectively, and subscripts e and f are be used to indicate the wavelengths of excitation and fluorescence, respectively. As in Fig. 3, the vertical levels corresponding to the top and the bottom of the mesophyll layer are 1 and 2. ChlF emitted from the leaf mesophyll layer can thus be described by the equations

$$F^-(2) = f E^-(1) + g E^+(2) \tag{11}$$

$$F^+(1) = g E^-(1) + f E^+(2) \tag{12}$$

After incorporating the leaf-air interfaces at the top and the bottom, we apply similar equations, in which we use double-primed fluorescence quantities and the vertical levels are 0 and 3 instead of 1 and 2:

$$F^-(3) = f''\, E^-(0) + g''\, E^+(3) \tag{13}$$

$$F^+(0) = g''\, E^-(0) + f''\, E^+(3) \tag{14}$$

As derived in Appendix C, the double-primed backward and forward fluorescence quantities are given by

$$f'' = X_e \left[(Y_e + Y_f) g + (1 + Y_e Y_f) f \right] X_f \tag{15}$$

$$g'' = X_e \left[(1 + Y_e + Y_f) g + (Y_e + Y_f) f \right] X_f \tag{16}$$

where

$$X_\lambda = \frac{t_{21\lambda}}{1 - r_{21\lambda} R_{b\lambda}}, \quad Y_\lambda = \frac{\tau_\lambda r_{21\lambda}}{1 - \rho_\lambda r_{21\lambda}}, \quad (\lambda = e, f). \tag{17}$$

It can be concluded that the effects of the border interfaces on the leaf mesophyll fluorescence matrices are easy to implement.

2.4. The doubling method

The doubling algorithm is a powerful tool for the calculation of radiative transfer in a homogeneous medium. It can easily be extended to include fluorescence and therefore it has been selected as the method applied in Fluspect to calculate the fluorescence matrices f and g of the leaf mesophyll layer.

In the doubling method we work with a small quantity ε, which represents the fraction of the total optical thickness of the layer to be simulated. If the whole layer is divided into a large number 2^n of thin and optically identical sub layers, then $\varepsilon = 2^{-n}$, where n is the number of doubling steps to be applied. When applied to the Kubelka-Munk differential equations, radiative transfer for a single layer without considering fluorescence is approximated by

$$E^-(1) = [1-(k+s)\varepsilon]E^-(0) + s\varepsilon E^+(1), \tag{18}$$

$$E^+(0) = s\varepsilon E^-(0) + [1-(k+s)\varepsilon]E^+(1) \tag{19}$$

where k is the absorption coefficient and s the backscattering coefficient. For a homogeneous and optically thick layer we may define the reflectance ρ and the transmittance τ by

$$E^-(b) = \tau E^-(t) + \rho E^+(b) \tag{20}$$

$$E^+(t) = \rho E^-(t) + \tau E^+(b) \tag{21}$$

where b and t indicate the bottom and the top of the layer, respectively. Since the Kubelka-Munk system has an analytical solution, the relationship between k and s on one hand and ρ and τ on the other is known and given by the equations

$$\rho = \frac{r_\infty(1-e^{-2m})}{1-r_\infty^2 e^{-2m}}; \qquad \tau = \frac{(1-r_\infty^2)e^{-m}}{1-r_\infty^2 e^{-2m}}, \tag{22}$$

$$\text{where } m = \sqrt{k(k+2s)} \text{ and } r_\infty = \frac{k+s-m}{s} = \frac{s}{k+s+m}. \tag{23}$$

However, in order to establish the starting equations (Eqs. (18) and (19)) of the doubling procedure, we need to derive the absorption and scattering coefficients k and s from given ρ and τ. The solution of this equation is given in Appendix B, and the result is given by

$$s = \frac{2a}{a^2-1}\ln b; \qquad k = \frac{a-1}{a+1}\ln b, \tag{24}$$

where

$$a = \frac{1+\rho^2-\tau^2+\sqrt{D}}{2\rho}; \qquad b = \frac{1-\rho^2+\tau^2+\sqrt{D}}{2\tau}; \tag{25}$$

$$D = (1-\rho+\tau)(1+\rho-\tau)(1-\rho-\tau)(1+\rho+\tau). \tag{26}$$

To include ChlF in the doubling algorithm, we express the hemispherical fluorescence for a single elementary layer at the start of the procedure by

$$\varphi = 0.5\eta\Phi(\lambda_f)k_{Chl}(\lambda_e)\sigma(\lambda_e,\lambda_f), \tag{27}$$

where η is the fluorescence quantum efficiency in radiation energy units, Φ is the fluorescence spectral distribution function in nm^{-1} at photosystem level, k_{Chl} is the absorption optical thickness, also taken as the excitation spectrum of the chlorophyll in the leaf mesophyll layer, and σ is a sigmoid function given by

$$\sigma(\lambda_e,\lambda_f) = \frac{1}{1+\exp\left[(\lambda_e-\lambda_f)/10\right]} \tag{28}$$

This function is used to suppress the so-called anti-Stokes fluorescence. It goes to zero if the wavelength of excitation largely exceeds the wavelength of fluorescence.

To incorporate fluorescence in the doubling method, for the fluorescence wavelength Eqs. (18) and 19 are modified into

$$F^-(1) = [1-(k_f+s_f)\varepsilon]F^-(0) + s_f\varepsilon F^+(1) + \varphi\varepsilon E^-(0) + \varphi\varepsilon E^+(1), \tag{29}$$

$$F^+(0) = s_f\varepsilon F^-(0) + [1-(k_f+s_f)\varepsilon]F^+(1) + \varphi\varepsilon E^-(0) + \varphi\varepsilon E^+(1), \tag{30}$$

and for the excitation wavelength we write as before

$$E^-(1) = [1-(k_e+s_e)\varepsilon]E^-(0) + s_e\varepsilon E^+(1), \tag{31}$$

$$E^+(0) = s_e\varepsilon E^-(0) + [1-(k_e+s_e)\varepsilon]E^+(1). \tag{32}$$

These equations form the basis under the doubling procedure with fluorescence included. A doubling step consists in combining two identical layers and calculating the reflectance, transmittance, backward fluorescence and forward fluorescence of the combined layer. With the initial equations, given by

$$r_\lambda = s_\lambda\varepsilon;\ \ t_\lambda = 1-(k_\lambda+s_\lambda)\varepsilon;\ \ f_\lambda = \varphi_\lambda\varepsilon;\ \ g_\lambda = \varphi_\lambda\varepsilon;\ \ (\lambda = e,f) \tag{33}$$

the resulting doubling step is expressed by

$$x_\lambda = \frac{t_\lambda}{1-r_\lambda^2}; \quad t'_\lambda = t_\lambda x_\lambda, \quad r'_\lambda = r_\lambda(1+t'_\lambda), \quad (\lambda = e,f). \tag{34}$$

$$f' = f(x_e+x_f) + gx_ex_f(r_e+r_f) \tag{35}$$

$$g' = g\left[1+x_ex_f(1+r_er_f)\right] + f(x_er_e+x_fr_f) \tag{36}$$

where the primed quantities refer to the newly formed double layer.

These equations, which are derived in Appendix A, are still relatively simple, which explains the high computational speed of the doubling algorithm for the calculation of fluorescence. A full calculation of the four excitation-fluorescence matrices (backward and forward matrices for both photosystems PS-I and PS-II) at 1 nm spectral resolution with Matlab takes only about 0.1 sec on an average PC. The optimum number of doubling steps depends on the machine floating point precision and the required accuracy. A small number of doubling steps leads to a low numerical precision in the approximation of the differential equations of radiative transfer. On the other hand, a large number of doubling steps leads to a very small value of ε, and for the given floating point machine precision this may lead to a relative inaccurate difference between the transmittance and unity at the start of the algorithm. For 32-bit floating point numbers it turns out that 15 doubling steps gives a fair compromise between both criteria mentioned.

2.5. Implementation of Fluspect in SCOPE

In this paper Fluspect is used independently, but for a broader understanding it is useful to briefly address the implementation of

Fluspect in the canopy radiative transfer and energy balance model SCOPE (Van der Tol et al., 2009). In SCOPE, Fluspect is executed first, and the output of reflectance, transmittance and ChlF matrices f and g are stored for later use in the radiative transfer and energy balance routines for the whole canopy. This procedure is accurate for reflectance and transmittance, as long as pigment concentrations and structure are uniform throughout the canopy. However, the ChlF matrices f' and g' are not uniform, because the fluorescence emission efficiencies η_{I} and η_{II} depend on the efficiency of competing quenching mechanisms of photochemical quenching (PQ) and non-photochemical quenching (NPQ), which in turn depend on quantities that vary in the canopy: leaf temperature, illumination and carboxylation capacity (Van der Tol et al., 2014). Because the matrices f' and g' scale linearly with η, it is not necessary to run Fluspect for all leaves separately. It is sufficient to correct f' and g' (of PS-II) for the effects of PQ and NPQ per leaf, by multiplying them by a coefficient $\eta_{\mathrm{II}}/\eta_{\mathrm{II}(0)}$ afterwards, where $\eta_{\mathrm{II}(0)}$ is the default value, and η_{II} is calculated as function of PQ and NPQ separately for each leaf in the canopy following Van der Tol et al. (2014). With the corrected f' and g', the ChlF emission by sunlit and shaded leaves of different orientation and optical depth in the canopy is calculated. The re-absorption and scattering of the emitted ChlF in the canopy is calculated by a separate radiative transfer routine (Van der Tol et al., 2009).

3. Methodology

We compared simulations of the Fluspect model to measurements of reflectance, transmittance and ChlF spectra for plants grown in a greenhouse. The experiment (Section 3.1) was designed to maximize between plant differences in pigment content. This enabled us to verify the simulated dependence of ChlF on pigment content using the procedure as sketched in Fig. 4: by first fitting the model to observed reflectance and transmittance, and next comparing simulated to observed ChlF (Section 3.2).

3.1. Experimental setup

A total number of 96 pots of barley (*Hordeum vulgare* L.) and sugar beet (*Beta vulgaris* L.) were grown in a greenhouse under controlled conditions in Forschungszentrum Jülich between December 2013 and March 2014. Because daylight hours were too short and many days were cloudy, the natural light was complemented with artificial light from growth lamps for 15 h per day, from 6 am to 9 pm, such that the total light intensity remained relatively stable throughout the day. The plants were grown under three different light conditions (16 pots per treatment per species). A portion of the pots was grown under full light conditions (HL treatment) with incoming photosynthetically active radiation (iPAR) of about 1000 µmol photons m^{-2} s^{-1} (measured in the greenhouse with Li-190SL), and the other two portions under reduced light, by covering them either with one (OC treatment, filtering out about 60% of full iPAR) or two layers of shade cloth (DC treatment, filtering out about 85% of full PPFD), to provoke differences in leaf pigment content and acclimation of photosynthesis to light conditions. When the plants were fully grown, a part of the pots grown under full light were exposed to water deficits (D treatment).

3.1.1. Reflectance, transmittance and chlorophyll fluorescence measurements

Measurements were taken on the leaves of intact plants using one or two healthy and fully developed leaves per pot. Due to insufficient growth of sugar beet under lower light intensities, measurements of sugar beet were only performed on plants grown in full light conditions. The measurements were carried out using artificial excitation light, except for one sunny day in March, when measurements were taken outdoor in full sunlight on a few high light (HL) adapted barley leaves and a few samples from the water deficit (D) group.

The setup consisted of a spectroradiometer (FieldSpec 4, ASD Inc.) connected to a FluoWat leaf clip (Alonso et al., 2007), through an optical fibre. The portable FluoWat leaf clip enables one to discriminate the emitted ChlF from the reflected and transmitted light by consecutive measurements using unfiltered and filtered incident light. A short-pass filter can be slotted into the opening for incident light, which cuts off the incoming light spectrum between 650 and 850 nm. We used a TechSpec OD4 short-pass filter (Edmund Optics GmbH, Germany). The leaf is positioned in the leaf clip, normally with its adaxial side facing the light source. The measurements are taken on either side of the leaf, such that the 'forward' and 'backward' ChlF signal (650 to 850 nm) are measured. A standard reflectance panel is used to estimate the incident (unfiltered, I) and the filtered (I_f) incident radiation and the exact transmittance of the filter. For more details on the FluoWat leaf clip, see Van Wittenberghe et al. (2013). The samples were illuminated by a cold light lamp (KL 2500 LCD, SCHOTT B.V., The Netherlands) as an artificial and constant light source to collect indoor measurements under 5 different light intensities, with iPAR ranging from 100 to 700 µmol photons m^{-2} s^{-1}. When measuring the spectra at different light intensities, we marked the position of the leaf clip on the leaf, to keep the measurement position constant. An example of the data obtained from the FluoWat is presented in Fig. 5. The transmittance of the filter (τ), the apparent (i.e. including fluorescence contribution) reflectance (R_{a}) and transmittance (T_{a}), the backward (F_{u}) and forward fluorescence (F_{d}) were calculated as

$$\tau = \frac{I_f}{I} \tag{37}$$

$$R_a = \frac{E_u}{I} \tag{38}$$

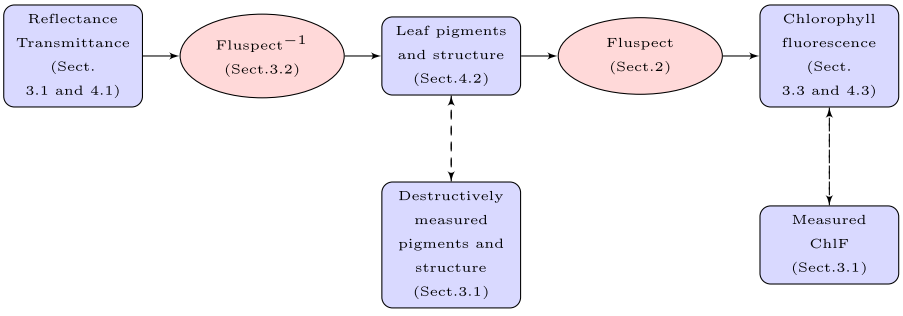

Fig. 4. Fluspect model evaluation process. Leaf pigment contents and structural properties were retrieved from reflectance and transmittance (the superscript '1' denotes model retrieval or inversion), followed by the simulation of ChlF. Both retrieved parameters and simulated ChlF were compared to measurements.

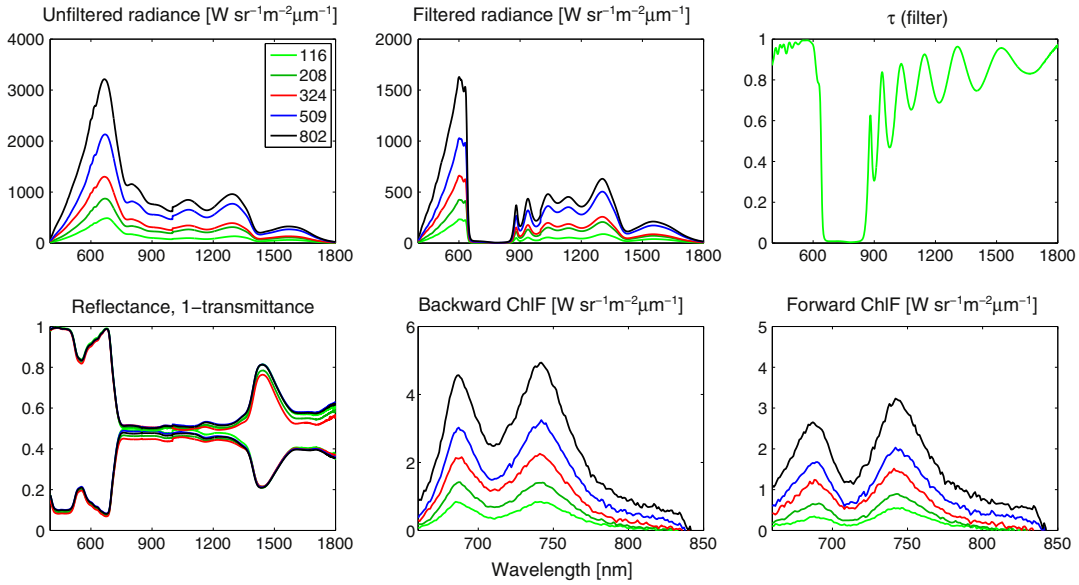

Fig. 5. Representation of a measurement sequence. Top from left to right: incident light at 5 intensities, incident filtered light, and the ratio between filtered and unfiltered incident light (the transmittance of the filter). Bottom from left to right: true reflectance and 1-transmittance, ChlF in the backward direction (i.e. from the top of the leaf), and ChlF in the forward direction.

$$T_a = \frac{E_d}{I} \tag{39}$$

$$F_u = \frac{E_{uf} - E_u\tau}{1-\tau} \tag{40}$$

$$F_d = \frac{E_{df} - E_d\tau}{1-\tau} \tag{41}$$

The true reflectance (R) and transmittance (T) were calculated as

$$R = R_a \quad \text{for wl} < 650 \quad \text{nm and for wl} > 850 \quad \text{nm} \tag{42}$$

$$R = R_a - F_u \quad \text{for} \quad 650 \quad \text{nm} < \text{wl} < 850 \quad \text{nm} \tag{43}$$

$$T = T_a \quad \text{for wl} < 650 \quad \text{nm for wl} > 680 \quad \text{nm} \tag{44}$$

$$T = T_a - F_u \quad \text{for} \quad 650 \quad \text{nm} < \text{wl} < 850 \quad \text{nm} \tag{45}$$

It should be noted that the measurements below 660 nm are unreliable due to the cut-off filter's characteristics. Between approximately 650 and 660 nm, the filter has an 'opening', which causes a sharp rise in the measured ChlF spectrum. Thus this is not ChlF, but a measurement artefact.

Unlike solar light, the artificial light was not fully collimated. This caused additional scattering in the opening of the FluoWat clip, which affected our estimate of the filter transmittance and thus ChlF. To correct for this contamination, we retrieved the true τ^* and a down-scaling factor α. Three additional measurements were taken at the intensity of about 700 µmol photons m^{-2} s^{-1}: white reference without filter while keeping the plastic holder on (I_h), white reference without filter and without the plastic holder (I_e) and white reference with the filter (I^*). These measurements were used to calculate the true τ^* and a down-scaling factor α:

$$\tau^* = \frac{I^*}{I_h} \tag{46}$$

$$\alpha = \frac{I_h}{I_e} \tag{47}$$

Finally, ChlF was retrieved:

$$F_u = \frac{E_{uf} - E_u \quad \alpha \quad \tau^*}{1-\tau^*} \tag{48}$$

$$F_d = \frac{E_{df} - E_d \quad \alpha \quad \tau^*}{1-\tau^*} \tag{49}$$

3.1.2. Destructive measurements of leaf biochemical and structural properties

We cut circles with diameter of 9 mm for further determination of specific leaf area (SLA [cm^2 mg^{-1}]), leaf water content (C_w [g cm^{-2}]), dry matter content (C_{dm} [g cm^{-2}]) and relative dry matter content (LDMC, leaf dry mass/fresh mass) of the sampled leaves. Total chlorophyll (C_{ab} [µg cm^{-2}]) and carotenoid (C_{car} [µg cm^{-2}]) content was determined with UV-VIS spectroscopy (Uvikon XL, Bio-tec instruments) by 100% acetone extraction according to Lichtenthaler and Buschmann (2001).

3.2. Retrieval of model parameters

We used reflectance and transmittance data of 23 barley leaves (of which 9 were also measured outdoors) and 11 sugar beet leaves, in the spectral range from 400 nm to 1800 nm for parameter retrieval. Data of each leaf sample were used separately in the model simulations.

The retrieved parameters were chlorophyll (C_{ab}), carotenoid (C_{car}), leaf water (C_w), dry matter (C_{dm}) and senescent material (C_s, brown pigments) content, and leaf mesophyll structure parameter (N). The two remaining parameters, notably fluorescence quantum efficiency for PS-I and PS-II (η_I and η_{II}), which have no effect on reflectance and transmittance, were retrieved separately.

The structural parameters were obtained after fitting the modelled R and T spectra to measurements at one light intensity (iPAR = 300 µmol photons m^{-2} s^{-1}). The two fluorescence quantum efficiency parameters, η_I and η_{II}, were retrieved at all light intensities,

while keeping structural parameters constant at their retrieved values. A trust-region algorithm was applied in Matlab using the built-in function 'lsqnonlin' to quantify a cost function. The stopping criteria were an insignificant change in parameter values and a minimum improvement in the cost function of 10^{-6}; iteration stopped when one of these criteria were met. The algorithm provided optimised parameters once for each leaf. The choice of starting values did not affect the result, indicating that local minima did not occur because the spectral effect of each parameter was sufficiently distinct. The following cost function was applied:

$$C = (M - S)^2 \tag{50}$$

where M is the measured spectrum in the form of a vector and S the corresponding simulation re-sampled to the resolution of the ASD FieldSpec 4 bands.

The parameters were retrieved by fitting just reflectance, just transmittance, and by fitting both at the same time. The results of the three alternative procedures were compared to each other. The retrieved parameter values were compared to corresponding destructive measurements of the same leaves by calculating the root mean-squared error (RMSE) and Pearson's correlation coefficients (R^2) as measures for the goodness-of-fit. It should be noted that this is only an indicative comparison as the parameters of a radiative transfer model may not be directly comparable to measurable quantities.

Error propagation in the retrieval of parameters and the simulation of ChlF was carried using the Jacobian (J) of the model. The uncertainty in the parameters ΔP was calculated from the standard deviation of the measured spectra ΔM as

$$\Delta P = (J_{RT} J_{RT}')^{-1} J_{RT}' \Delta M \tag{51}$$

where J_{RT} is a matrix with the partial derivatives of the reflectance or transmittance at each wavelength (rows) to each parameter (columns). The uncertainty in the simulated ChlF was calculated from ΔP as

$$\Delta F = J_F \Delta P \tag{52}$$

where J_F is a matrix with the partial derivatives of the ChlF at each wavelength (rows) to each parameter (columns).

3.3. Backward and forward chlorophyll fluorescence simulations

The optimised parameters obtained at a light intensity of iPAR = 300 µmol photons m^{-2} s^{-1} by fitting both R and T simultaneously, were further used to simulate forward and backward ChlF at all light intensities. The filtered incident light spectrum of each measurement was provided as the incident light input parameter. In these simulations it was assumed that the emission efficiency of ChlF was a constant, hence η_{I} and η_{II} for photosystems I and II were kept constant. We maintained them at the default values for both species: 0.001 and 0.02, for η_{I} and η_{II}, respectively. Because these efficiencies were kept constant, the simulated ChlF should be proportional to the illumination intensity. Comparison between measured and modelled ChlF at different light intensities then reveals possible variations in emission efficiency.

Simulated and measured spectra of ChlF at the two peaks were compared to each other by calculating the RMSE and R^{-2}. Next, differences between treatments were evaluated for both species. In case of comparing two treatments, HL and D, a two-tailed t-test was used. Comparison between all treatments for barley was performed by using a one-way ANOVA test.

As a final step, the efficiencies η_{I} and η_{II} were fitted to each observation of ChlF separately at all light intensities, by including the measured ChlF spectra in the cost function. During this procedure, we kept other parameter values constant at optimised values obtained at a light intensity of iPAR = 300 µmol photons m^{-2} s^{-1} by fitting both R and T simultaneously. This enabled us to investigate, how the emission efficiencies vary between the species, treatment, light intensity, and with light quality (i.e. artificial light versus natural solar light).

4. Results and discussion

In this section we compare measured and simulated reflectance and ChlF spectra (obtained for both artificial and natural sunlight), measured and retrieved PROSPECT parameters, and we evaluate the model performance to reproduce variations in ChlF due to variations in PROSPECT parameters.

4.1. Reflectance and transmittance

In Table 2 we show the RMSE in-between the spectra measured at 5 different light intensities, and between the simulated spectrum and the 5 measured spectra, for both species. For this comparison, spectra were divided into 3 bands: VIS (400–700 nm), NIR1 (700–1000 nm, which is where the range of the second detector of the ASD ends) and NIR2 (1000–1800 nm).

The RMSEs between measured spectra indicate the reproducibility of the measurements. The low values in the VIS (less than 0.025) indicate good reproducibility. However, the RMSEs in the NIR regions display values up to 0.09, possibly either due to measurement error or the artificial light's properties. In the NIR region of some measurements, the sum of R and T spectra exceeds one. Leaves with either a higher quantity of trichoma or/and an increased cuticle thickness are known to have a non-Lambertian reflectance (Slaton et al., 2001; Woolley, 1971). This effect, together with scattering within the chamber may have been responsible for an overestimate of R. When tuning simultaneously for both R and T spectrum, this overestimate may cause an inaccurate estimation of model parameters that affect reflectance in the NIR region, notably C_{s} and C_{w}. The effect on C_{ab} and C_{car}, which were of most interest for this study, is limited.

The RMSEs of modelled compared to measured spectra indicate the model performance. The spectral RMSEs for the VIS are generally less than 0.03, indicating good spectrum reconstruction (Jacquemoud et al., 1996) for both reflectance and transmittance. Also, the values are generally comparable to RMSEs between measurements, indicating that the model fit was acceptable. It should be noted that fitting the model does not result in an exact match between model and measurements. This is due to the fact that the optical properties of the absorbing materials (C_{ab}, C_{dm} etc.) are prescribed inputs spectra of the model. They were not tuned to the measurements, and therefore, some spectral mismatch can remain after retrieving the concentrations (but not the spectral shapes) of the absorbing materials.

An example of measured reflectance and transmittance spectra, optimised for either reflectance and transmittance or both simultaneously, is represented in Fig. 6. The measured spectra show typical characteristics of a plant leaf, with R and T being low in the VIS and high in the NIR region. The two leaves compared in the figure differ in C_{ab} concentrations. The leaf with lower C_{ab} concentration has higher R and T in the VIS region. The general effects of leaf pigment content and leaf structure on R and T of leaves has been extensively studied before (Demarez, 1999; Gitelson et al., 1998, 2003) and complies with our findings, but is not the focus of this study.

Table 2
(a) RMSE of measured reflectance (R) and transmittance (T) spectra shown for all leaves of barley and sugar beet, measured indoors. Spectra measured at 5 different light intensities were compared to the spectrum measured at 200 µmol photons m^{-2} s^{-1}, (b) RMSE of simulated compared to measured (at iPAR = 200 µmol photons m^{-2} s^{-1}) R and T spectra. The following spectral regions were distinguished: VIS (400–700 nm), NIR1 (700–1000 nm, which is where the range of the second detector of the ASD ends) and NIR2 (1000–1800 nm).

Band	Spectrum (a)	Barley	Sugar beet (b)	Barley	Sugar beet
VIS (400–700 nm)	R	0.025	0.018	0.032	0.023
	T	0.018	0.011	0.022	0.015
lNIR1 (700–1000 nm)	R	0.089	0.083	0.076	0.082
	T	0.094	0.077	0.080	0.074
NIR2 (1000–1800 nm)	R	0.079	0.073	0.070	0.074
	T	0.094	0.073	0.084	0.074

4.2. Parameter retrievals

Parameters obtained by destructive analysis (C_{ab}, C_{car}, C_{dm} and C_w) were compared to the attributable retrieved PROSPECT parameters (Fig. 7). Supporting statistical data is shown in Table 3. Retrieved PROSPECT C_{ab} parameter for barley is in a strong agreement with destructive measurements for barley (R^2 ranges from 0.69 to 0.75 with RMSE of approximately 3 to 5.5 µg cm^{-2} for the three tuning options). On the other hand, the R^2 for sugar beet reaches a maximum value of only 0.36, most likely due to the narrow range of variation of experimental data. However, RMSEs are similar for both species. Compared to other parameter retrieval methods, our results for barley provide a fairly good estimate for C_{ab} concentrations, with encouragingly low RMSE values. Different approaches, for example PROSPECT inversion according to Demarez (1999) and Jacquemoud et al. (1996) and a regression algorithm based on the Gaussian Processes by Van Wittenberghe et al. (2014), gave similar results for goodness-of-fit and the RMSE values for retrieved versus measured C_{ab} concentrations.

The retrievals of C_{car} values were fairly good, especially when outdoor samples were included in the calculations (Table 3, 'All samples'): R^2 is 0.6, when optimising for T and R simultaneously. Retrieved C_w is underestimated and the measured variability is not reproduced (see low R^2 in Table 3 and the clusters of C_w in Fig. 7). Similar holds for retrieved C_{dm} and for many samples the retrieval of C_{dm} failed completely. However, for outdoor measurements all retrievals were successful. We attribute the failed retrievals to the measurement error of both spectral (explained in Section 4.1) and destructive measurements. The reliability of the destructive C_w and C_{dm} measurements is limited, as dry matter and water content are difficult to measure accurately in practice, due to the impact of sample preparation, rehydration procedure and time of collection (Garnier et al., 2001; Turner, 1981).

Leaf senescent material (C_s) and leaf mesophyll structure parameter (N) were also retrieved. Information on average values of retrieved parameters can be found in Table 9. C_s was on average approximately 0.06 for barley leaves (with the exception of OC group) and 0.09 for sugar beet leaves. The two species differed significantly in the leaf structure parameter N, with average treatment values ranging from 1.53–1.6 for barley and 1.43–1.46 for sugar beet leaves. Generally, N ranging between 1 and 1.5 corresponds to monocotyledons (in this case barley) and between 1.5 and 2.5 corresponds to dicotyledons (sugar beet) (Jacquemoud and Baret, 1990). Thus, sugar beet values of N fall slightly below the expected values, which could be due to both specific growing conditions and leaf immaturity.

The statistical analysis in Table 3 gave best general results for parameters obtained by optimising for R and T simultaneously and we use these results for ChlF spectra simulations in further evaluation of the model.

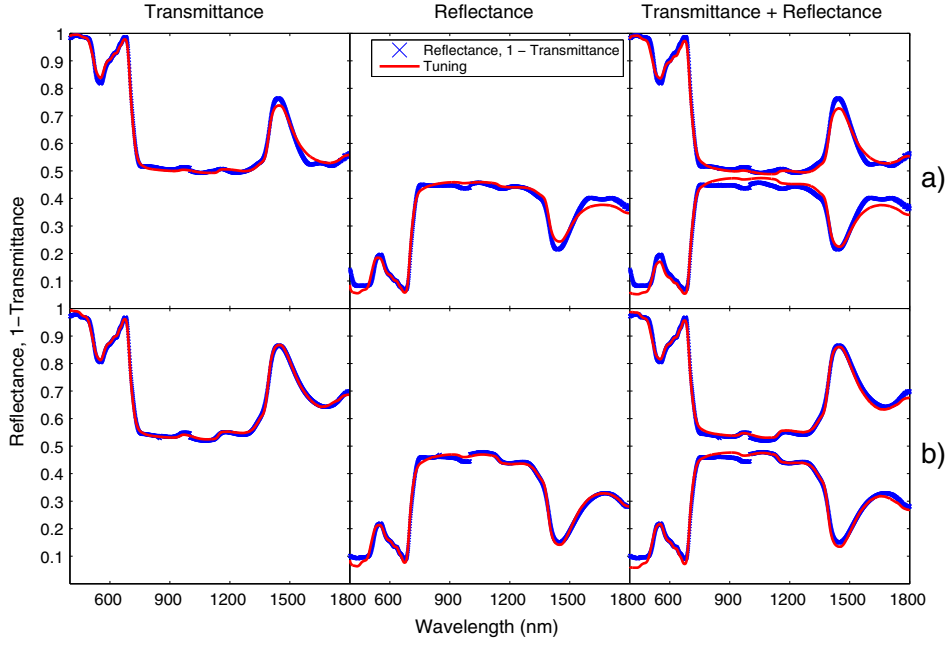

Fig. 6. Reflectance and transmittance spectra, where parameters were optimised to best reproduce measured transmittance, reflectance, or both simultaneously, for one barley leaf (a) grown at high light, with measured ChlF concentration of C_{ab} = 35 µg cm^{-2}, measured under iPAR = 328 µmol photons m^{-2} s^{-1}), and (b) grown under double cloth, with measured ChlF concentration of C_{ab} = 18 µg cm^{-2}, measured under iPAR = 344 µmol photons m^{-2} s^{-1}).

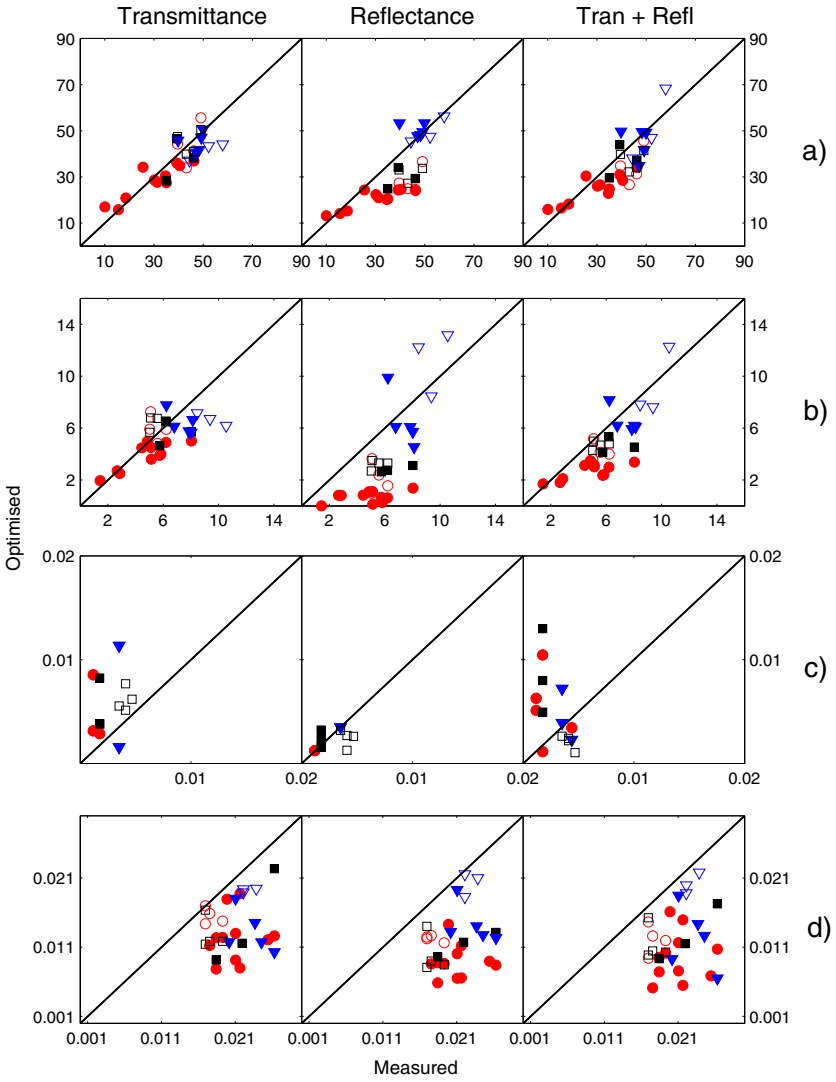

Fig. 7. Optimised PROSPECT parameters versus the measured (from destructive sampling) equivalents: (a) chlorophyll (C_{ab} [μg cm^{-2}]) and (b) carotenoid (C_{car} [μg cm^{-2}]) concentrations; (c) dry matter (C_{dm} [g cm^{-2}]) and (d) leaf water (C_w [cm]) content; represented for two species: barley measured indoors (red circles), barley measured outdoors (black squares) and sugar beet (blue triangles). Empty symbols represent reduced soil moisture samples). Parameters were optimised to best reproduce measured transmittance, reflectance, or both simultaneously. (For interpretation of the references to color in this figure legend, the reader is referred to the web version of this article.)

4.3. Simulated chlorophyll fluorescence

Fig. 8 shows ChlF spectra for two leaves (the leaves shown in Fig. 6, namely high and low C_{ab}), both with default values of η (left) and with η tuned for each sample separately. Applying the default values of η, the red peak of ChlF is reproduced fairly well, but the far-red peak is underestimated, especially for backward ChlF. These over and underestimates partly disappear after tuning η, but some

Table 3
Statistical data supporting Fig. 7. R^2 and RMSE are represented per species and for all samples (including barley leaves measured outdoors) for each of the optimised Fluspect parameters versus their measured equivalents (C_{ab} [μg cm^{-2}], C_{car} [μg cm^{-2}], C_{dm} [g cm^{-2}], C_w [cm]). C_{dm} is shown for all samples only. Parameters were optimised to best reproduce measured transmittance, reflectance, or both simultaneously.

		Transmittance		Reflectance		Tran + Refl	
		R^2	RMSE	R^2	RMSE	R^2	RMSE
Barley	C_{ab}	0.75	5.4	0.71	3.2	0.69	4.5
	C_{car}	0.42	1.1	0.08	0.9	0.29	0.8
	C_w	0.03	0.0034	0.10	0.0025	0.02	0.0035
Sugar beet	C_{ab}	0.03	4.4	0.12	3.8	0.36	8.8
	C_{car}	0.08	0.7	0.21	3.1	0.41	1.8
	C_w	0.17	0.0038	0.13	0.0038	0.12	0.0055
All samples	C_{ab}	0.69	5.9	0.55	8.6	0.64	7.0
	C_{car}	0.40	1.1	0.51	2.5	0.60	1.4
	C_{dm}	0.12	0.0033	0.05	0.0012	0.02	0.0070
	C_w	0.02	0.0037	0.04	0.0040	0.03	0.0043

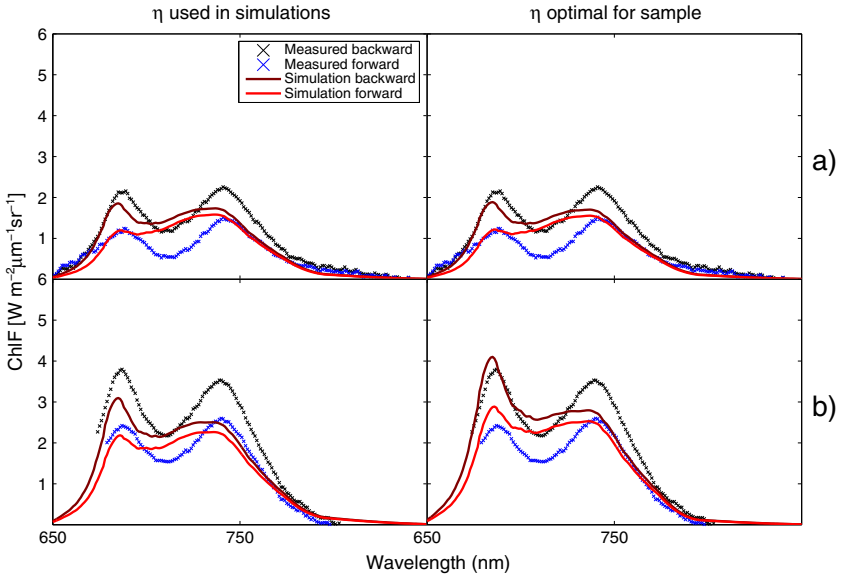

Fig. 8. ChlF spectra at incoming PAR of about 300 μmol photons m^{-2} s^{-1} for one barley leaf grown (a) at high light level with estimated ChlF concentration of $C_{ab} = 35$ μg cm^{-2}, and (b) under a double cloth with estimated ChlF concentration of $C_{ab} = 18$ μg cm^{-2}. PROSPECT parameters were optimised to best reproduce both measured reflectance and transmittance. Simulations were performed using either the default values of η (left), or η optimised for each sample separately (right): η_I and η_{II}, for (a) 0.0018 and 0.0102; for (b) 0.0014 and 0.0135, respectively.

discrepancies remain; for example, the underestimation of the far-red peak, the shallower valley between the two peaks and a somewhat narrower red peak.

The higher red peak for the lower C_{ab} leaf confirms that red ChlF is re-absorbed (Van Wittenberghe et al., 2015). We expected that by tuning the emission efficiencies, the underestimate of the far-red ChlF would disappear, because the two peaks are scaled separately: η_I affects the far-red peak and η_{II} mostly the red peak (Franck et al., 2002). However, this proved not to be the case. The remaining underestimate of the far-red peak after tuning η suggests that there is a problem with the shape of the emission spectra. Another explanation for the underestimate could be the measurement conditions; in particular, the effect that the different spectral quality of the incoming light might have on a leaf, compared to that of solar light.

In Fig. 9, we show the relationship between measured and simulated ChlF at the two peaks (690 nm and 740 nm) at three light intensities for all samples. For each leaf, we retrieved a separate set of model parameters from R and T at one light intensity, but the emission efficiency parameters (η) were kept constant at default values, for PS-I and PS-II, respectively. In Fig. 9, we present HL, OC and DC treatments for barley collectively, whereas samples exposed to reduced soil moisture (D) are presented separately due to the fact that they differed most from all other samples (analysed using one-way ANOVA, not shown).

ChlF is better reproduced for the red peak than far-red peak for both species, as already suggested in Fig. 8 and supported by the degree of agreement between measured and simulated values (with R^2 ranging from 0.18 to 0.99 for 690 nm peak compared to R^2 ranging from 0.02 to 0.98 for 760 nm peak) presented in Table 4. Moreover, results in Table 4 indicate that model predictions are generally better for forward ChlF. This is to be expected, as the light passing through the leaf interacts more with the inner leaf structure than reflected light, in contrast to reflected light and backward ChlF, which are mostly affected by the upper layers (Van Wittenberghe et al., 2015), where leaf anatomy might play a more significant role in light propagation.

The agreement between backward measured and simulated ChlF varies: for sugar beet they are in a high agreement (R^2 ranges from a minimum of 0.53 for 740 nm peak to 0.88 for 690 nm peak), in contrast to barley, where R^2 reaches a maximum of 0.38, where only indoor samples are considered. However, at the highest light intensity (Fig. 9c), where barley measured outdoors is shown together with indoors HL samples only, the combined R^2 reaches 0.98. Moreover, the inclusion of barley outdoor samples generally improves the agreement between the simulations and measurements, for both forward and backward ChlF.

Thus for sugar beet, we can explain most of the variability of ChlF emission at the top and bottom of the leaf from the six PROSPECT biochemical and structural parameters alone (keeping emission efficiency at the photo-system level constant) (Gitelson et al., 1998; Jacquemoud et al., 1996; Van Wittenberghe et al., 2015). On the other hand, for barley leaves, PROSPECT parameters do not explain the variations in ChlF, when all experimental treatments of indoor measurements are combined in the analysis. The magnitude of simulated backward ChlF for barley samples measured indoors is significantly lower than that of the measurements, and the simulations show less variability.

4.3.1. Relations between experimental treatments

In Fig. 9, we can observe an apparent difference in ChlF between reduced soil moisture samples (D) and all other samples. The reduced soil moisture samples were selected from the plants grown under high light (HL), and were later exposed to reduced soil moisture. These samples appear to show significantly different values for the PROSPECT parameters than the HL samples (Table 5). The simulated and measured ChlF are also significantly different between HL and D for barley (Table 6), but for sugar beet, the significant difference in ChlF is only reproduced for the backward flux.

In Table 5 we show the differences in PROSPECT parameters between groups. For barley, differences in chlorophyll and carotenoid concentrations explain most of variation between treatments. The average C_{ab} and C_{car} concentrations of the D samples was higher than that of the HL samples (Table 9). This is contrary to what we expected, and suggests that other factors, such as leaf development with age or Julian date (the D samples were measured later),

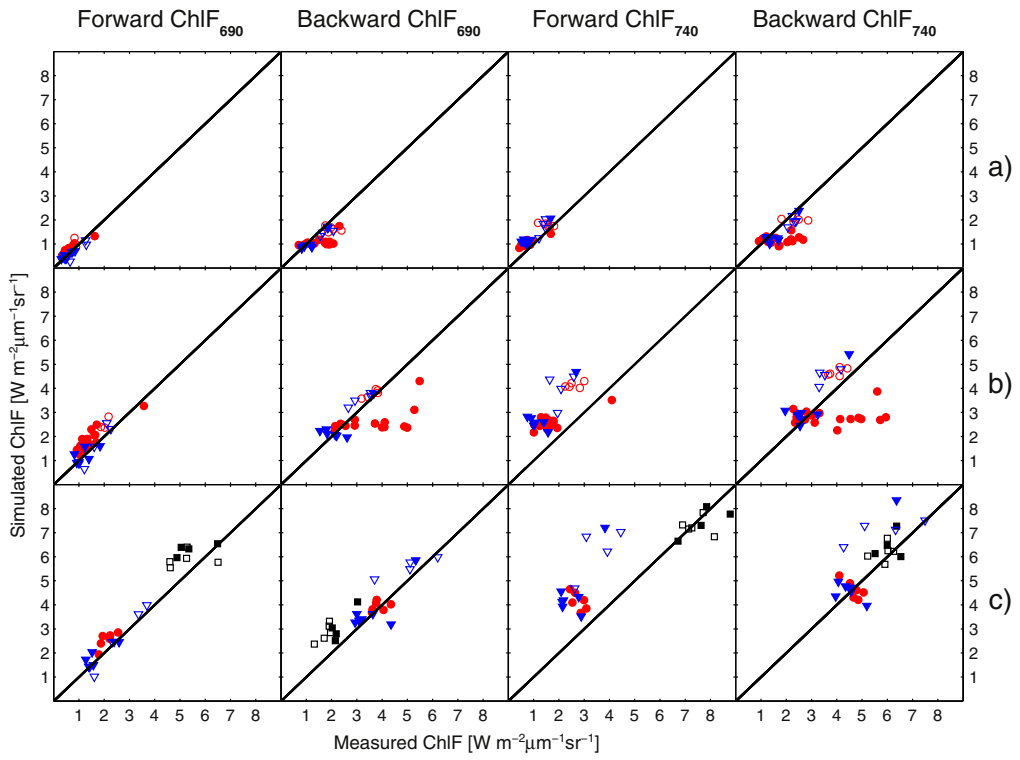

Fig. 9. Modelled versus measured backward and forward ChlF at 690 and 740 nm for three light intensities (approximated): (a) 200, (b) 500 and (c) 700–800 µmol photons (m^{-2}) (s^{-1}); for two species: barley measured indoors (red circles; only HL represented at (c)), barley measured outdoors (black squares; only represented at (c)) and sugar beet (blue triangles). Empty symbols represent reduced soil moisture samples. Note that for each indoors sample all model parameters were fixed at the optimised values for one light intensity, and the emission efficiency parameters (η) for both photosystems were kept constant. (For interpretation of the references to color in this figure legend, the reader is referred to the web version of this article.)

may have caused the differences in biochemical and structural properties between the treatments rather than drought stress. However, regardless of the explanation for the differences between HL and D samples, the model reproduces these differences accurately.

4.3.2. The role of the emission efficiency parameters

As mentioned previously, the emission efficiency parameters (η) for both photosystems were initially kept constant, in order to evaluate the effects of leaf biochemical and structural properties.

Table 4
Statistical data supporting Fig. 9. R^2 and RMSE are represented for all samples (including barley leaves measured outdoors) and by species for each light intensity. Data was modelled from optimised parameters for both transmittance (T) and reflectance (R) simultaneously; each was evaluated separately, namely as 'Forward' and 'Backward'. All model parameters were fixed at the optimised values at one light intensity for each sample.

		Forward						Backward					
		Barley		Sugar beet		All samples		Barley		Sugar beet		All samples	
		R^2	RMSE	R^2	RMSE	R^2	RMSE	R^2	RMSE	R^2	RMSE	R^2	RMSE
$ChlF_{690}$	$iPAR_{200}$	0.73	0.11	0.81	0.13	0.59	0.16	0.38	0.23	0.88	0.13	0.50	0.22
	$iPAR_{500}$	0.79	0.23	0.72	0.34	0.67	0.34	0.18	0.60	0.76	0.41	0.26	0.60
	$iPAR_{750}$	0.99	0.11	0.90	0.32	0.93	0.38	0.99	0.15	0.73	0.65	0.96	0.50
$ChlF_{740}$	$iPAR_{200}$	0.76	0.16	0.82	0.19	0.76	0.18	0.25	0.33	0.83	0.21	0.37	0.33
	$iPAR_{500}$	0.59	0.46	0.61	0.61	0.50	0.56	0.02	0.84	0.76	0.54	0.06	0.90
	$iPAR_{750}$	0.97	0.34	0.68	0.83	0.86	1.04	0.98	0.33	0.53	1.11	0.95	0.72

Table 5
Differences in PROSPECT parameters between treatments of barley and sugar beet: plants grown under full sunlight (HL), plants grown under one shade cloth (OC), plants grown under double shade cloth (DC), plants grown under full sunlight exposed to reduced soil moisture (D); result of a t-test. Level of significance is represented by *** for $p \leq 0.001$, ** for $p > 0.001$ and $p \leq 0.01$, * for $p > 0.01$ and $p > 0.05$ and – for no significance.

	Compared groups		C_{ab}	C_{car}	C_w	C_{dm}	C_s	N
Barley	HL	OC	–	–	–	–	–	–
	HL	DC	*	***	–	–	–	–
	HL	D	*	*	–	–	–	–
	OC	DC	*	*	–	–	–	–
	OC	D	*	**	–	–	–	–
	DC	D	***	***	–	–	–	–
Sugar beet	HL	D	–	–	*	–	–	–

Table 6
Differences in the two peaks of ChlF spectra (s - simulated, m - measured) at three different light intensities (iPAR), for barley and sugar beet, as a result of exposing the plants grown under full sunlight (HL) to reduced soil moisture (D); result of a t-test. Level of significance is represented by *** for p≤ 0.001, ** for p>0.001 and p≤ 0.01, * for p> 0.01 and p> 0.05 and – for no significance.

				Backward				Forward			
				$ChlF_{690s}$	$ChlF_{690m}$	$ChlF_{740s}$	$ChlF_{740m}$	$ChlF_{690s}$	$ChlF_{690m}$	$ChlF_{740s}$	$ChlF_{740m}$
Barley	$iPAR_{200}$	HL	D	***	***	***	***	*	***	***	***
	$iPAR_{300}$	HL	D	***	***	***	***	*	**	***	***
	$iPAR_{500}$	HL	D	***	***	***	***	*	**	***	***
Sugar beet	$iPAR_{200}$	HL	D	*	**	*	*	–	*	–	*
	$iPAR_{300}$	HL	D	*	*	–	*	–	*	–	*
	$iPAR_{500}$	HL	D	**	*	*	–	–	*	–	–

To study the potential effect of fluorescence emission efficiency values (η), we further optimised these two parameters by minimizing the RMSE between simulated and measured ChlF, and compared fitted η values to model default values ($\eta_{II} = 0.01$ and $\eta_I = 0.002$, with a ratio of 1:5) based on work of Miller et al. (2005). In general, both photosystems (PS-I and PS-II) contribute to the ChlF signal, but PS-II causes most of the variability in the signal, contributing to both red and far-red ChlF emission, while PS-I contributes up to 35% in the form of far-red light (Palombi et al., 2011).

In Table 7, we explore the significance of differences in η values between treatments. In most comparisons for barley, η_{II} differs significantly between treatments, whereas changes in η_I are less evident. Thus, most of variability is due to η_{II}, which supports our initial assumption. Interestingly, η_I is significantly different between HL and D samples. However, for sugar beet samples, the results are less clear, with varied differences between HL and D treatments in both parameters for the light intensities.

These results are further supported by the results shown in Table 8, where average retrieved values for various treatments are presented and clear differences between treatments can also be observed. This suggests that different treatments not only lead to differences in leaf structure and pigment content, but also in leaf physiology; as revealed by the emission efficiencies.

4.3.3. Relation between chlorophyll fluorescence and chlorophyll concentration

We further focus on the role of Chl concentration, which we expected to account for most of the variability of ChlF.

In Fig. 10, we show the relation of simulated and measured ChlF to the increasing chlorophyll concentrations of the leaves. To represent the overall relationship between ChlF and C_{ab} in the model, we also plotted a simulation of ChlF versus C_{ab}, increasing from 1 to 90 µg cm^{-2} in steps of 1, while keeping all other parameters constant.

Forward red ChlF shows a typical decline with chlorophyll content (Gitelson et al., 1998; Pedrós et al., 2010). This effect is due to increasing chlorophyll re-absorption in the red with higher C_{ab} concentrations (Agati et al., 1993; Gitelson et al., 1998; Van Wittenberghe et al., 2014).

Barley samples again show much higher variations than sugar beet. We note that concurrent photosynthesis measurements (data not shown) showed that sugar beet, unlike barley, was unstressed and showed high photosynthesis rates, which might explain the higher agreement between measured and simulated ChlF. A link between increased ChlF variability and a physiological down-regulation of leaf photosynthesis was also reported by Schickling etal. (2016). Moreover, barley plants were grown under various light intensities, thus they not only differ in chlorophyll concentrations, but also in the physiology and anatomy of the leaves.

Table 7
Differences in efficiency parameters (η_I and η_{II}) between treatments over three different light intensities (iPAR) for barley and sugar beet as a result of a one-way ANOVA. As the differences are minimal, only $iPAR_{300}$ for barley is shown. Level of significance is represented by *** for p≤ 0.001, ** for p>0.001 and p≤ 0.01, * for p> 0.01 and p> 0.05 and – for no significance.

	Light intensity	Compared groups		η_I	η_{II}
Barley	$iPAR_{300}$	HL	OC	–	***
		HL	DC	–	***
		HL	D	**	***
		OC	DC	–	–
		OC	D	–	***
		DC	D	–	**
Sugar beet	$iPAR_{200}$	HL	D	–	*
	$iPAR_{300}$	HL	D	–	*
	$iPAR_{500}$	HL	D	–	–

4.3.4. Effect of illumination quantity

In both the measured and simulated ChlF spectra shown in Fig. 9, ChlF levels increase significantly with increasing light intensity, as expected (Gitelson et al., 1998; Van Wittenberghe et al., 2014). However, analysis of changes in η_I and η_{II} with increasing light intensity, either in general or within experimental groups, revealed no variability. The range of illumination intensity (200–800 µmol photons m^{-2} s^{-1}) was either too small, or the experimental design was not suitable to draw any conclusion on the effect of illumination intensity on η. Consequently, these results are not reported in this paper.

4.3.5. Effect of illumination quality

Plant ontogenesis and plant spectral response at any period of development are known to be greatly affected by the properties of the light source (Gitelson et al., 1998; Hogewoning et al., 2010). Fluspect simulates the excitation wavelength dependence of ChlF through radiative transfer equations, but the spectral shapes of emission by the PS-I and PSI-II are independent of the excitation wavelength (except that anti-Stokes radiation is suppressed). An open question remains whether the spectral shape of the artificial light source causes any physiological responses that are not accounted for by the model.

To address this question, we compared measurements recorded under full sunlight and under artificial light in the laboratory (Fig. 11). These measurements were collected for the same leaf, within 24 h of each other, to reduce the potential change in the structural and biochemical properties of the leaves.

Assuming that leaf biochemical and structural properties remained the same, we simulated *R*, *T* and ChlF for both leaves, using the PROSPECT parameters retrieved for indoor measurements. Since η_I and η_{II} might have changed between measurements, we used values that were optimised for each leaf separately. The model resembles spectra measured under natural sunlight better than those measured under artificial light.

Although *R* and *T* spectra were similar (the same leaf was measured), the measurements show a relatively high red peak in the artificial light induced ChlF compared to the SIF. For the same emission efficiencies, the model would predict an almost identical spectral

Table 8
Average tuned values for photosystems I (η_I) and II (η_{II}) and their ratios for the following: (a) four barley groups (HL - high light, OC - one cloth, DC - double cloth, D - reduced soil moisture), two sugar beet groups (HL - high light, D - reduced soil moisture) illuminated by artificial light; and (b) the difference between barley leaves of two treatments, measured outdoors under natural illumination.

	Barley					Sugar beet				
Setup	η_I	SD	η_{II}	SD	Ratio $\eta_{II}/_I$	η_I	SD	η_{II}	SD	Ratio $\eta_{II}/_I$
HL	$1.5 \cdot 10^{-3}$	$4.8 \cdot 10^{-4}$	$7.9 \cdot 10^{-3}$	$1.3 \cdot 10^{-3}$	5.3	$1.2 \cdot 10^{-3}$	$3.0 \cdot 10^{-4}$	$8.1 \cdot 10^{-3}$	$1.5 \cdot 10^{-3}$	6.7
OC	$1.3 \cdot 10^{-3}$	$4.3 \cdot 10^{-4}$	$14.7 \cdot 10^{-3}$	$1.0 \cdot 10^{-3}$	11.1	–	–	–	–	–
DC	$1.3 \cdot 10^{-3}$	$1.6 \cdot 10^{-4}$	$14.1 \cdot 10^{-3}$	$1.2 \cdot 10^{-3}$	10.6	–	–	–	–	–
D	$0.7 \cdot 10^{-3}$	$2.5 \cdot 10^{-4}$	$10.9 \cdot 10^{-3}$	$0.7 \cdot 10^{-3}$	15.8	$0.7 \cdot 10^{-3}$	$5.1 \cdot 10^{-4}$	$10.5 \cdot 10^{-3}$	$0.3 \cdot 10^{-3}$	14.3
HL_{out}	$2.8 \cdot 10^{-3}$	$2.1 \cdot 10^{-4}$	$6.8 \cdot 10^{-3}$	$0.8 \cdot 10^{-3}$	2.4	–	–	–	–	–
D_{out}	$2.8 \cdot 10^{-3}$	$0.6 \cdot 10^{-4}$	$6.8 \cdot 10^{-3}$	$1.1 \cdot 10^{-3}$	2.4	–	–	–	–	–

Table 9
Average values of tuned parameters used for ChlF simulations and the error propagation in the retrieval of parameters expressed as (±) RMSE for each parameter, expressed as percentage of the parameter.

Species	Sample	C_{ab}	%	C_{dm}	%	C_w	%	C_s	%	C_{car}	%	N	%
Barley	HL	28.6±3.9	3.3	$0.002 \pm 3.4 \cdot 10^{-3}$	114.5	$0.009 \pm 3.6 \cdot 10^{-3}$	6.0	0.059±0.09	64.7	2.9±0.37	4.6	1.57±0.12	2.3
	OC	27.9±1.7	1.7	$0.001 \pm 1.5 \cdot 10^{-3}$	162.3	$0.009 \pm 3.3 \cdot 10^{-3}$	1.7	0	–	2.6±0.37	3.7	1.56±0.07	2.2
	DC	17.4±1.2	4.4	$0.004 \pm 3.3 \cdot 10^{-3}$	71.9	$0.012 \pm 5.8 \cdot 10^{-3}$	7.8	0.068±0.11	81.0	1.8±0.20	11.8	1.53±0.15	2.0
	D	37.1±7.2	2.2	$0.002 \pm 4.4 \cdot 10^{-3}$	30.9	$0.012 \pm 1.9 \cdot 10^{-3}$	2.8	0.061±0.08	49.6	3.5±0.62	3.6	1.59±0.07	3.8
Sugar beet	HL	46.1±6.7	3.4	$0.003 \pm 2.9 \cdot 10^{-3}$	56.4	$0.011 \pm 4.0 \cdot 10^{-3}$	4.6	0.090±0.11	40.5	6.0±0.87	4.2	1.43±0.10	6.6
	D	48.4±6.7	0.9	$0.011 \pm 4.9 \cdot 10^{-3}$	4.7	$0.018 \pm 3.9 \cdot 10^{-3}$	1.3	0.089±0.08	49.1	7.9±0.94	1.2	1.47±0.09	8.4

shape of the ChlF curves. In reality, the spectral shape of the artificial light may have favoured PS-II ChlF, as indicated by the retrieved values of η.

By comparing optimised η values for the two settings (Table 8), we found that the ratio η_{II}/η_I is lower outdoors (2.4) than in the laboratory (5.3), mostly because η_{II} was lower outdoor. This indicates that there are other spectral effects not accounted for by the model.

4.4. Model sensitivity analysis

As mentioned in Section 3.2, we used a Jacobian (J) of the model for determination of error propagation of the R and T measurements into the retrieved parameters and the simulation of ChlF. We investigated how a small change (a step of the size 10^{-6}) in the model parameters propagates into the simulated reflectance and transmittance. The resulting Jacobian was then used to translate the RMSE of the measured reflectance and transmittance at various light intensities into RMSEs of the parameters (Table 9). The RMSEs are expressed as percentages of the average values of the tuned parameters.

The scale of error ranges from a few percent up to almost 160% for the barley dry matter parameter. C_s and C_{dm} have by far the greatest uncertainty for both species.

In the next step (Fig. 12), we investigated how the uncertainty in retrieved model parameters propagated into the simulation of ChlF spectra. It appears that the propagated uncertainty in ChlF is small (see the shaded area's in Fig. 12). C_s and C_{dm} contribute most to the variability, in particular for the drought (D) and one cloth shaded (OC) treatment. The retrieved values for these two parameters were uncertain, but this is compensated for by the limited sensitivity of

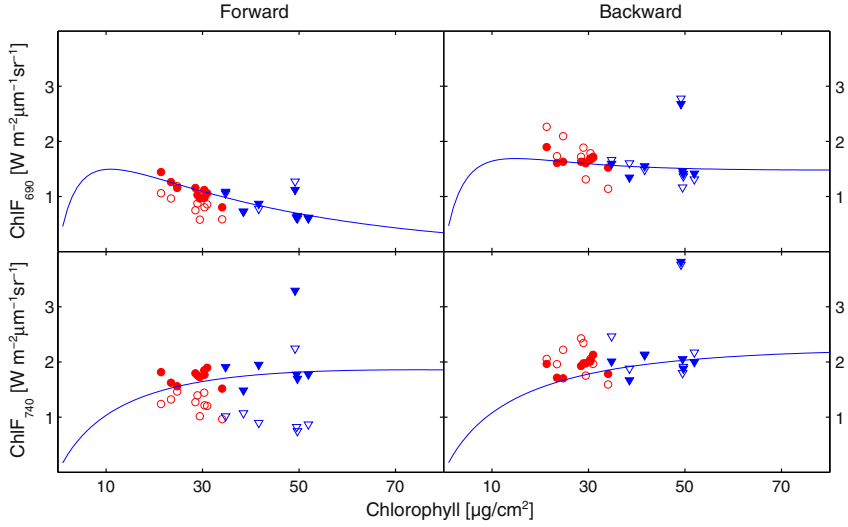

Fig. 10. Modelled and measured forward and backward ChlF at 690nm and at 740nm versus the optimised Fluspect parameter C_{ab} for light intensity at 300 µmol photons m^{-2} s^{-1} for the two species (barley (circles) and sugar beet (triangles)). Empty symbols represent measured values and full symbols simulated values. The blue curve represents modelled ChlF versus chlorophyll concentrations, while keeping all other model parameters fixed at the values of one representative barley leaf grown in high light.

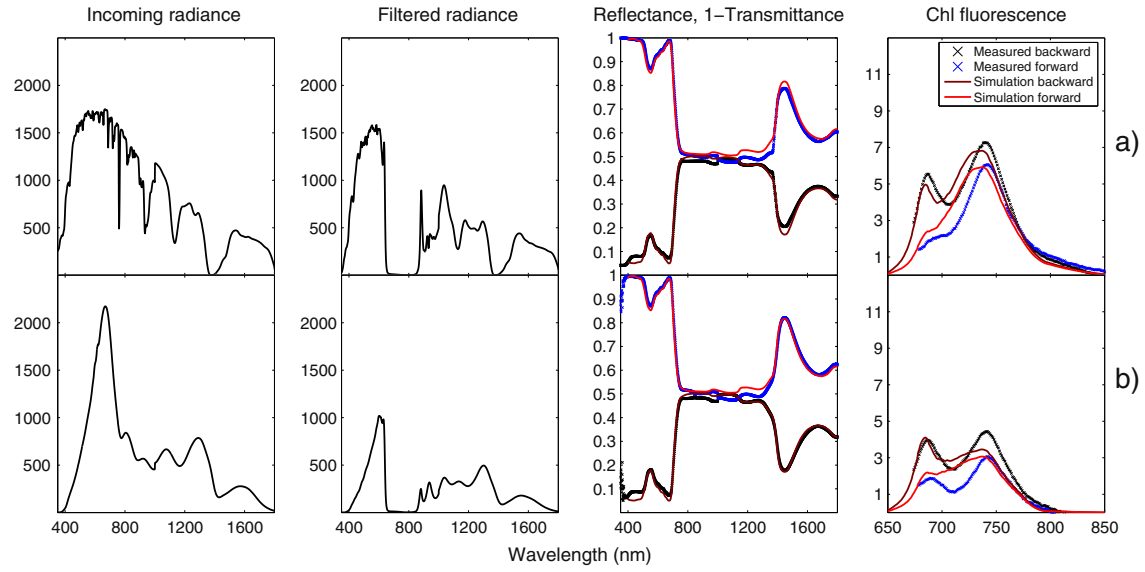

Fig. 11. Comparison between measured incoming unfiltered and filtered radiation, modelled and measured reflectance, transmittance and ChlF spectra for one barley leaf measured: (a) outside under natural illumination of iPAR = 682 µmol photons (m^{-2}) (s^{-1}), η_{I} and η_{II} are 0.0027 and 0.0068, respectively; (b) in the laboratory under artificial illumination of iPAR = 526 µmol photons m^{-2} s^{-1}, η_{I} and η_{II} are 0.0005 and 0.0095, respectively. For both simulations, we used PROSPECT parameters optimised for leaf (b), with C^{ab} = 31 µg cm^{-2}. Incoming radiance and ChlF are expressed in W (sr^{-1} m^{-2}µm^{-1}).

ChlF to these two parameters. However, the opposite is the case for C_{ab}: ChlF is rather sensitive to C_{ab}, which was estimated accurately. In both cases, the propagated uncertainty of ChlF is small.

5. Conclusions

We have presented the Fluspect-B model, a computationally fast radiative transfer model that calculates leaf reflectance, transmittance, and ChlF emission spectra between 640 nm and 850 nm from excitation spectra from 400 to 700 nm.

Parameter retrieval for leaf chlorophyll and carotenoid concentrations works reasonably well, particularly for transmittance. However, we note that the retrieval could be further improved by improving the specific absorption coefficients of leaf biochemical components.

The model was able to reproduce observed variations in ChlF from the retrieved (PROSPECT) parameters, in particular: (1) the increase of ChlF with increasing radiance, and (2) the decrease of forward red ChlF with chlorophyll content. Simulations agreed more with measurements for the red peak and for forward simulations, than for the far-red peak and backward simulations.

Furthermore, fluorescence emission efficiency parameters hold potential additional information about dynamic behaviour of photosynthesis, as shown by differences in retrieved emission efficiencies.

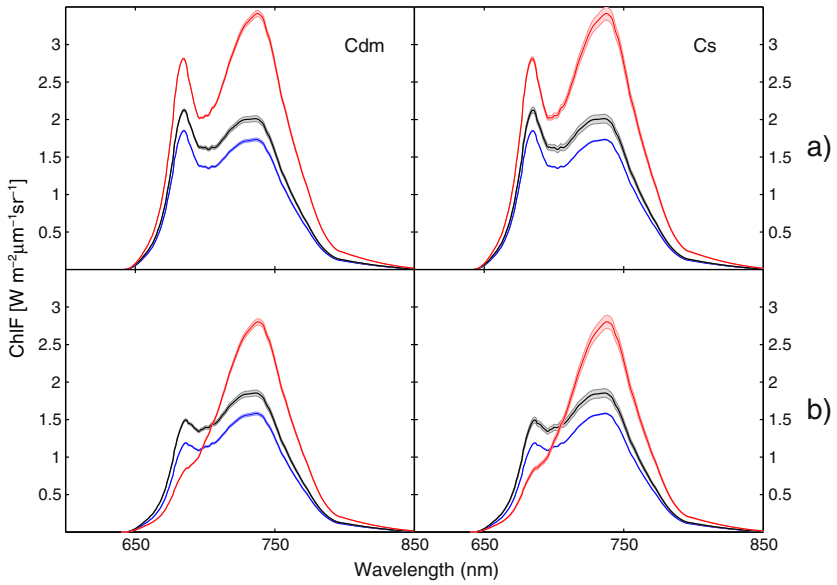

Fig. 12. Influence of error propagation in the retrieval of parameters on (a) backward and (b) forward ChlF simulations. Results are presented for one representative barley leaf for C_s and C_{dm}: top (red) - D, middle (black) - OC, bottom (blue) - HL) samples. The shaded area shows the RMSE caused by the RMSE in each parameter value. (For interpretation of the references to color in this figure legend, the reader is referred to the web version of this article.)

However, we could not explore this in further detail due to limitations of the experimental data.

Our measurements were carried out mostly under artificial light; a few measurements were carried out using sunlight as the excitation source. It appears that the model reproduces the outdoor measurements more accurately. The spectral distribution of the excitation light appears to affect the shape of the measured ChlF spectrum in a way that the model cannot fully reproduce. After the calibration of PROSPECT parameters and fluorescence emission efficiencies, some systematic differences between the measured and simulated shapes of the ChlF spectra still remain. These are unrelated to the radiative transfer scheme, and rather suggest that the initial PS-I and PS-II emission spectra used in the model need to be improved. This improvement would also preferably be done by taking high quality, SIF measurements.

We conclude that leaf biochemical and structural properties have a substantial effect on ChlF and that Fluspect-B is able to reproduce these effects. Fluspect-B model is also computationally efficient, which makes it possible to simulate reflectance and ChlF spectra of whole vegetation canopies in a radiative transfer scheme such as SCOPE. By means of inversions, biochemical and structural properties together with fluorescence emission efficiencies could then be retrieved from field and airborne data of ChlF and reflectance.

Acknowledgement

The research presented in this paper is funded by the Netherlands Organisation for Scientific Research(NWO) in the frame of the Earth and Life Sciences (ALW) division, project ALW-GO/13-32. Additional funding for model development was provided by the European Space Agency (ESA), FLEX/Sentinel-3 Tandem Mission Photosynthesis Study (ESA/ESTEC Contract No. 4000106396/12/NL/AF) and FLEX/Sentinel-3 Tandem Mission Bridge Study ESA/ESTEC Contract No. 4000112341/14/NL/FF/gp). The authors thank Hella Ahrends for her organizational efforts, Marijke van der Tol for her help with the measurements and Edelgard Schölgens for laboratory analyses.

Appendix A. Border effects on fluorescence

In order to calculate the effective fluorescent emission from the complete leaf, we assume that the only incident flux is the forward excitation flux at the top interface, $E^-(0)$. In this case we use the following equations to derive the incident fluxes on the leaf's mesophyll layer (see also Fig. 3).

$$E^-(1) = t_\alpha E^-(0) + r_{21}E^+(1) \tag{A.1}$$

$$E^+(1) = \rho E^-(1) + \tau E^+(2) \tag{A.2}$$

$$E^-(2) = \tau E^-(1) + \rho E^+(2) \tag{A.3}$$

$$E^+(2) = r_{21}E^-(2) \tag{A.4}$$

From the latter two of these equations we obtain first

$$(1-\rho r_{21})E^-(2) = \tau E^-(1), \tag{A.5}$$

and next we obtain the pair of equations

$$E^-(1) - r_{21}E^+(1) = t_\alpha E^-(0) \tag{A.6}$$

$$-\rho E^-(1) + E^+(1) = \tau r_{21}E^-(2) = \frac{\tau^2 r_{21}}{1-\rho r_{21}}E^-(1) \tag{A.7}$$

Here the second equation gives the reflectance of the lowest two layers together, R_b, since one can write

$$E^+(1) = \left[\rho + \frac{\tau^2 r_{21}}{1-\rho r_{21}}\right]E^-(1) = R_b E^-(1). \tag{A.8}$$

We can now write

$$(1-r_{21}R_b)E^-(1) = t_\alpha E^-(0), \tag{A.9}$$

so

$$E^-(1) = \frac{t_\alpha}{1-r_{21}R_b}E^-(0) = XE^-(0), \tag{A.10}$$

where

$$X = \frac{t_\alpha}{1-r_{21}R_b}, \tag{A.11}$$

and which is the forward flux incident at the top of the mesophyll layer.

Since

$$(1-\rho r_{21})E^-(2) = \tau E^-(1), \tag{A.12}$$

we find

$$E^-(2) = \frac{\tau}{1-\rho r_{21}}E^-(1) = \frac{\tau}{1-\rho r_{21}}XE^-(0), \tag{A.13}$$

and finally

$$E^+(2) = r_{21}E^-(2) = \frac{\tau r_{21}t_\alpha}{(1-\rho r_{21})(1-r_{21}R_b)}E^-(0) = YXE^-(0), \tag{A.14}$$

where

$$Y = \frac{\tau r_{21}}{1-\rho r_{21}} \tag{A.15}$$

which gives the backward flux incident on the bottom of the mesophyll layer.

At the fluorescence wavelength the following equations are applied:

$$F^+(1) = gE^-(1) + fE^+(2) + \rho F^-(1) + \tau F^+(2) \tag{A.16}$$

$$F^-(2) = fE^-(1) + gE^+(2) + \tau F^-(1) + \rho F^+(2) \tag{A.17}$$

$$F^+(2) = r_{21}F^-(2) \tag{A.18}$$

$$F^-(1) = r_{21}F^+(1) \tag{A.19}$$

Substitution of the second pair of equations in the first pair gives

$$F^+(1) = gE^-(1) + fE^+(2) + \rho r_{21}F^+(1) + \tau r_{21}F^-(2), \tag{A.20}$$

$$F^-(2) = fE^-(1) + gE^+(2) + \tau r_{21}F^+(1) + \rho r_{21}F^-(2). \tag{A.21}$$

and next we find

$$(1-\rho r_{21})F^+(1) - \tau r_{21}F^-(2) = gE^-(1) + fE^+(2) = P, \tag{A.22}$$

$$-\tau r_{21}F^+(1) + (1-\rho r_{21})F^-(2) = fE^-(1) + gE^+(2) = Q. \quad (A.23)$$

The solution is given by

$$F^+(1) = \frac{(1-\rho r_{21})P + \tau r_{21}Q}{(1-\rho r_{21})^2(\tau r_{21})} = \frac{P+YQ}{(1-\rho r_{21})(1-Y^2)}, \quad (A.24)$$

$$F^-(2) = \frac{\tau r_{21}P + (1-\rho r_{21})Q}{(1-\rho r_{21})^2(\tau r_{21})} = \frac{YP+Q}{(1-\rho r_{21})(1-Y^2)}. \quad (A.25)$$

Substitution of P and Q finally gives

$$F^+(1) = \frac{(g+Yf)E^-(1) + (f+Yg)E^+(2)}{(1-\rho r_{21})(1-Y^2)}, \quad (A.26)$$

$$F^-(2) = \frac{(Yg+f)E^-(1) + (Yf+g)E^+(2)}{(1-\rho r_{21})(1-Y^2)}. \quad (A.27)$$

The final fluorescence outputs at the top and the bottom of the leaf are

$$F^+(0) = t_{21}F^+(1) \quad (A.28)$$

$$F^-(3) = t_{21}F^-(2) \quad (A.29)$$

In order to derive the effective fluorescence coefficients, first the internal fluxes at the excitation wavelength have to be expressed in the incident flux $E^-(0)$, and next the above equations are used to determine the new fluorescence coefficients, which are called f' and g'. To make a clearer distinction between the wavelengths of excitation and fluorescence, in the following we will use the subscripts e and f. So we write

$$E^-(1) = X_eE^-(0), \quad (A.30)$$

$$E^+(2) = Y_eX_eE^-(0) \quad (A.31)$$

and

$$F^+(1) = \frac{(g+Y_ff)E^-(1) + (f+Y_fg)E^+(2)}{(1-\rho_f r_{21f})(1-Y_f^2)}, \quad (A.32)$$

$$F^-(2) = \frac{(Y_fg+f)E^-(1) + (Y_ff+g)E^+(2)}{(1-\rho_f r_{21f})(1-Y_f^2)}. \quad (A.33)$$

Since the effective fluorescence coefficients are defined by

$$F^-(3) = f'E^-(0), \quad (A.34)$$

$$F^+(0) = g'E^-(0), \quad (A.35)$$

it follows that

$$g' = \frac{(g+Y_ff)X_e + (f+Y_fg)Y_eX_e}{(1-\rho_f r_{21f})(1-Y_f^2)t_{21f}} = X_e\frac{(1+Y_fY_e)g + (Y_e+Y_f)f}{(1-\rho_f r_{21f})(1-Y_f^2)t_{21f}}, \quad (A.36)$$

$$f' = \frac{(Y_fg+f)X_e + (Y_ff+g)Y_eX_e}{(1-\rho_f r_{21f})(1-Y_f^2)t_{21f}} = X_e\frac{(Y_e+Y_f)g + (1+Y_fY_e)f}{(1-\rho_f r_{21f})(1-Y_f^2)t_{21f}}. \quad (A.37)$$

Some further simplification is still possible since, in general,

$$1 - r_{21}R_b = 1 - r_{21}\left[\rho + \frac{\tau^2 r_{21}}{1-r_{21}\rho}\right] = 1 - r_{21}\rho - \frac{\tau^2 r_{21}^2}{1-r_{21}\rho} \quad (A.38)$$

$$= (1-r_{21}\rho)\left[1 - \frac{\tau^2 r_{21}^2}{(1-r_{21}\rho)}\right] = (1-r_{21}\rho)(1-Y^2). \quad (A.39)$$

This implies that

$$X_f = \frac{t_{21f}}{(1-\rho_f r_{21})(1-Y_f^2)} = \frac{t_{21f}}{1-r_{21}R_b}, \quad (A.40)$$

and thus one can finally write

$$g' = X_e[(1+Y_eY_f)g + (Y_e+Y_f)f]X_f, \quad (A.41)$$

$$f' = X_e[(Y_e+Y_f)g + (1+Y_eY_f)f]X_f. \quad (A.42)$$

Appendix B. Derivation of Kubelka-Munk parameters k and s

In order to derive k and s from given values of ρ and τ, we first establish that, from Eq. (23),

$$r_\infty^{-1} - r_\infty = \frac{2m}{s} \text{and} r_\infty^{-1} + r_\infty = \frac{2(k+s)}{s} = 2\frac{k}{s} + 2, \quad (B.1)$$

from which we obtain

$$s = \frac{2m}{r_\infty^{-1} - r_\infty} \quad \text{and} \quad (B.2)$$

$$2\frac{k}{s} = r_\infty^{-1} - 2 + r_\infty = r_\infty^{-1}(1 - 2r_\infty + r_\infty^2) = \frac{(1-r_\infty)^2}{r_\infty}, \quad (B.3)$$

so

$$k = \frac{m}{r_\infty^{-1} - r_\infty}\frac{(1-r_\infty)^2}{r_\infty} = m\frac{(1-r_\infty)^2}{1-r_\infty^2} = m\frac{1-r_\infty}{1+r_\infty}. \quad (B.4)$$

In order to obtain m and r_∞, we first introduce the auxiliary quantities a and b defined by

$$a = r_\infty^{-1} \quad \text{and} \quad b = e^m. \quad (B.5)$$

Then one can write

$$\rho = \frac{a^{-1}(1-b^{-2})}{1-a^{-2}b^{-2}} = \frac{ab^2-a}{a^2b^2-1}; \quad \tau = \frac{(1-a^{-2})b^{-1}}{1-a^{-2}b^{-2}} = \frac{a^2b-b}{a^2b^2-1} \quad (B.6)$$

The sum and the difference give

$$\rho + \tau = \frac{ab^2 - a + a^2b - b}{a^2b^2-1} = \frac{(ab-1)(a+b)}{(ab-1)(ab+1)} = \frac{a+b}{ab+1}; \quad (B.7)$$

$$\rho - \tau = \frac{ab^2 - a - a^2b + b}{a^2b^2-1} = \frac{(-ab-1)(a-b)}{(ab-1)(ab+1)} = \frac{a-b}{-ab+1}. \quad (B.8)$$

From these equations we obtain

$$a + b = (\rho+\tau)(1+ab) = \rho + \tau + \rho ab + \tau ab; \quad (B.9)$$

$$a - b = (\rho-\tau)(1-ab) = \rho - \tau - \rho ab + \tau ab, \quad (B.10)$$

and next, again by summation and subtraction, one finds the important relationships

$$a = \rho + \tau ab; \tag{B.11}$$

$$b = \tau + \rho ab. \tag{B.12}$$

The product of these equations gives

$$ab = \rho\tau + (\rho^2 + \tau^2)ab + \rho\tau a^2 b^2. \tag{B.13}$$

From this quadratic equation in ab we can solve the product as

$$\begin{aligned} ab &= \frac{1 - \rho^2 - \tau^2 \pm \sqrt{(1 - \rho^2 - \tau^2)^2 - 4(\rho\tau)^2}}{2\rho\tau} \\ &= \frac{1 - \rho^2 - \tau^2 \pm \sqrt{D}}{2\rho\tau}. \end{aligned} \tag{B.14}$$

where

$$\begin{aligned} D &= (1 - \rho^2 - \tau^2)^2 - 4(\rho\tau)^2 \\ &= (1 - \rho^2 - \tau^2 + 2\rho\tau)(1 - \rho^2 - \tau^2 - 2\rho\tau) \\ &= [1 - (\rho - \tau)^2][1 - (\rho + \tau)^2] \\ &= (1 - \rho + \tau)(1 + \rho - \tau)(1 - \rho - \tau)(1 + \rho + \tau) \end{aligned} \tag{B.15}$$

Finally, we use Eqs. (B.11) and B.12 again to obtain a and b separately as

$$a = \rho + \tau ab = \rho + \frac{1 - \rho^2 - \tau^2 \pm \sqrt{D}}{2\rho} = \frac{1 + \rho^2 - \tau^2 \pm \sqrt{D}}{2\rho}; \tag{B.16}$$

$$b = \tau + \rho ab = \tau + \frac{1 - \rho^2 - \tau^2 \pm \sqrt{D}}{2\tau} = \frac{1 - \rho^2 + \tau^2 \pm \sqrt{D}}{2\tau}. \tag{B.17}$$

The product of the two solutions for a equals

$$\begin{aligned} &\frac{1 + \rho^2 - \tau^2 + \sqrt{D}}{2\rho} \frac{1 + \rho^2 - \tau^2 - \sqrt{D}}{2\rho} = \\ &= \frac{(1 + \rho^2 - \tau^2)^2 - [(1 - \rho^2 - \tau^2)^2 - 4(\rho\tau)^2]}{4\rho^2} \\ &= \frac{[(1 + \rho^2 + \tau^2) + (1 - \rho^2 - \tau^2)]}{4\rho^2} \\ &\quad \cdot \frac{[(1 + \rho^2 - \tau^2) - (1 - \rho^2 - \tau^2) - (1 - \rho^2 - \tau^2)] + 4(\rho\tau)^2}{4\rho^2} \\ &= \frac{4(1 - \tau^2)\rho^2 + 4\rho^2\tau^2}{4\rho^2} = 1 \end{aligned} \tag{B.18}$$

The same holds for those of b. Since, according to their given definitions, both a and b are greater than or equal to unity, we have to select the greater of the two solutions as the correct ones in both cases, i.e.

$$a = \frac{1 + \rho^2 - \tau^2 + \sqrt{D}}{2\rho}; b = \frac{1 - \rho^2 + \tau^2 + \sqrt{D}}{2\tau}. \tag{B.19}$$

Expressing s and k in terms of a and b finally gives

$$s = \frac{2a}{a^2 - 1} \ln b; k = \frac{a - 1}{a + 1} \ln b. \tag{B.20}$$

Appendix C. Derivation of doubling equations with fluorescence included

Writing for the optical quantities of the single elementary layer at the start of the doubling sequence

$$r = s\varepsilon; \tag{C.1}$$

$$t = 1 - (k + s)\varepsilon; \tag{C.2}$$

$$f = \varphi\varepsilon; \tag{C.3}$$

$$g = \varphi\varepsilon, \tag{C.4}$$

we can write for the top layer of two identical layers

$$F^-(1) = t_f F^-(0) + r_f F^+(1) + f'' E^-(0) + g'' E^+(1) \tag{C.5}$$

$$F^+(0) = r_f F^-(0) + t_f F^+(1) + g'' E^-(0) + f'' E^+(1) \tag{C.6}$$

$$E^-(1) = t_e E^-(0) + r_e E^+(1) \tag{C.7}$$

$$E^+(0) = r_e E^-(0) + t_e E^+(1) \tag{C.8}$$

For an optically identical bottom layer we get the similar equations

$$F^-(2) = t_f F^-(1) + r_f F^+(2) + f'' E^-(1) + g'' E^+(2) \tag{C.9}$$

$$F^+(1) = r_f F^-(1) + t_f F^+(2) + g'' E^-(1) + f'' E^+(2) \tag{C.10}$$

$$E^-(2) = t_e E^-(1) + r_e E^+(2) \tag{C.11}$$

$$E^+(1) = r_e E^-(1) + t_e E^+(2) \tag{C.12}$$

A doubling step consists in combining the two above systems of equations in order to obtain new effective quantities describing the optical properties of the two layers added together. This is achieved by eliminating the fluxes at the interface between the two layers, i.e. those at level 1. For the purpose of deriving the doubling equations it is sufficient to assume that there is only one incident flux, namely $E^-(0)$. Then, at the excitation wavelength, we can write

$$E^-(1) - r_e E^+(1) = t_e E^-(0), \tag{C.13}$$

$$-r_e E^-(1) + E^+(1) = 0, \tag{C.14}$$

with the solutions

$$E^-(1) = \frac{t_e}{1 - r_e^2} E^-(0), \tag{C.15}$$

$$E^+(1) = \frac{r_e t_e}{1 - r_e^2} E^-(0). \tag{C.16}$$

Next the equations for the outgoing fluxes at levels 0 and 2 are used, giving

$$E^-(2) = \frac{t_e^2}{1 - r_e^2} E^-(0) \tag{C.17}$$

$$E^+(0) = \left[r_e + \frac{r_e t_e^2}{1 - r_e^2} \right] E^-(0) \tag{C.18}$$

From these we obtain the doubling equations for the reflectance and the transmittance at the excitation wavelength. We can write

$$x_e = \frac{t_e}{1 - r_e^2}; t'_e = t_e x_e; r'_e = r_e(1 + t'_e), \tag{C.19}$$

where the primed quantities refer to the newly formed double layer.

For the fluorescence wavelength we obtain similar equations. To obtain the effective fluorescence matrices, we also have to find the fluorescent fluxes at level 1. For this we use the equations

$$F^-(1) = r_f F^+(1) + f E^-(0) + g E^+(1), \tag{C.20}$$

$$F^+(1) = r_f F^-(1) + g E^-(1), \tag{C.21}$$

giving

$$F^-(1) - r_f F^+(1) = \left[f + g \frac{r_e t_e}{1 - r_e^2} \right] E^-(0) = (f + g x_e r_e) E^-(0), \tag{C.22}$$

$$-r_f F^-(1) + F^+(1) = g \frac{t_e}{1 - r_e^2} E^-(0) = g x_e E^-(0). \tag{C.23}$$

From these equations we obtain

$$F^-(1) = \frac{f + g x_e r_e + r_f g x_e}{1 - r_f^2} E^-(0), \tag{C.24}$$

$$F^+(1) = \frac{(f + g x_e r_e) r_f + g x_e}{1 - r_f^2} E^-(0). \tag{C.25}$$

Substitution of these in the equations for the outgoing fluorescent fluxes at levels 0 and 2 gives

$$\begin{aligned} F^+(0) &= t_f F^+(1) + g E^-(0) + f E^+(1) \\ &= \left[g + \frac{(f + g x_e r_e) r_f + g x_e}{1 - r_f^2} t_f + \frac{f r_e t_e}{1 - r_e^2} \right] E^-(0) \\ &= \left[g[1 + x_e x_f (1 + r_e r_f)] + f(x_e r_e + x_f r_f) \right] E^-(0), \end{aligned} \tag{C.26}$$

and

$$\begin{aligned} F^-(2) &= t_f F^-(1) + f E^-(1) \\ &= \left[\frac{f + g x_e r_e + r_f g x_e}{1 - r_f^2} t_f + f \frac{t_e}{1 - r_e^2} \right] E^-(0) \\ &= [f(x_e + x_f) + g x_e x_f (r_e + r_f)] E^-(0). \end{aligned} \tag{C.27}$$

These results imply that the doubling equations for the forward and backward fluorescence are given by, respectively,

$$g' = g[1 + x_e x_f (1 + r_e r_f)] + f(x_e r_e + x_f r_f), \tag{C.28}$$

$$f' = f(x_e + x_f) + g x_e x_f (r_e + r_f). \tag{C.29}$$

References

Ač, A., Malenovský, Z., Olejníčková, J., Gallé, A., Rascher, U., Mohammed, G., 2015. Meta-analysis assessing potential of steady-state chlorophyll fluorescence for remote sensing detection of plant water, temperature and nitrogen stress. Remote Sens. Environ. 168, 420–436. http://dx.doi.org/10.1016/j.rse.2015.07.022.

Agati, G., Fusi, F., Mazzinghi, P., di Paola, M.L., 1993. A simple approach to the evaluation of the reabsorption of chlorophyll fluorescence spectra in intact leaves. J. Photochem. Photobiol., B 17, 163–171. http://dx.doi.org/10.1016/1011-1344(93)80009-X.

Allen, W., Gausman, H., Richardson, A., 1970. Mean effective optical constants of cotton leaves. JOSA 60, 542–547.

Allen, W., Gausman, H., Richardson, A., Thomas, J., 1969. Interaction of isotropic light with a compact plant leaf. JOSA 59, 1376–1379.

Alonso, L., Gomez-Chova, L., Vila-Frances, J., Amoros-Lopez, J., Guanter, L., Calpe, J., Moreno, J., 2007. Sensitivity analysis of the Fraunhofer line discrimination method for the measurement of chlorophyll fluorescence using a field spectroradiometer. 2007 IEEE International Geoscience and Remote Sensing Symposiumpp. 3756–3759. http://dx.doi.org/10.1109/IGARSS.2007.4423660.

Buschmann, C., Nagel, E., 1993. In vivo spectroscopy and internal optics of leaves as basis for remote sensing of vegetation. Int. J. Remote Sens. 14, 711–722. http://dx.doi.org/10.1080/01431169308904370.

Campbell, P.K.E., Middleton, E.M., Corp, L.A., Kim, M.S., 2008. Contribution of chlorophyll fluorescence to the apparent vegetation reflectance. Sci. Total Environ. 404, 433–439. http://dx.doi.org/10.1016/j.scitotenv.2007.11.004.

Cogliati, S., Rossini, M., Julitta, T., Meroni, M., Schickling, A., Burkart, A., Pinto, F., Rascher, U., Colombo, R., 2015. Continuous and long-term measurements of reflectance and sun-induced chlorophyll fluorescence by using novel automated field spectroscopy systems. Remote Sens. Environ. 164, 270–281. http://dx.doi.org/10.1016/j.rse.2015.03.027.

Dawson, T.P., Curran, P.J., Plummer, S.E., 1998. LIBERTY—Modeling the effects of leaf biochemical concentration on reflectance spectra. Remote Sens. Environ. 65, 50–60.

Demarez, V., 1999. Seasonal variation of leaf chlorophyll content of a temperate forest. Inversion of the PROSPECT model. Int. J. Remote Sens. 20, 879–894. http://dx.doi.org/10.1080/014311699212975.

Demmig, B., Winter, K., Krüger, A., Czygan, F., 1987. Photoinhibition and zeaxanthin formation in intact leaves a possible role of the xanthophyll cycle in the dissipation of excess light energy. Plant Physiol.

Dobrowski, S.Z., Pushnik, J.C., Zarco-Tejada, P.J., Ustin, S.L., 2005. Simple reflectance indices track heat and water stress-induced changes in steady-state chlorophyll fluorescence at the canopy scale. Remote Sens. Environ. 97, 403–414. http://dx.doi.org/10.1016/j.rse.2005.05.006.

Eullaffroy, P., Vernet, G., 2003. The F684/F735 chlorophyll fluorescence ratio: a potential tool for rapid detection and determination of herbicide phytotoxicity in algae. Water Res. 37, 1983–1990. http://dx.doi.org/10.1016/S0043-1354(02)00621-8.

Feret, J.B., François, C., Asner, G.P., Gitelson, A.A., Martin, R.E., Bidel, L.P.R., Ustin, S.L., le Maire, G., Jacquemoud, S., 2008. PROSPECT-4 and 5: Advances in the leaf optical properties model separating photosynthetic pigments. Remote Sens. Environ. 112, 3030–3043.

Franck, F., Juneau, P., Popovic, R., 2002. Resolution of the Photosystem I and Photosystem II contributions to chlorophyll fluorescence of intact leaves at room temperature. Biochim. Biophys. Acta Biomembr. 1556, 239–246. http://dx.doi.org/10.1016/S0005-2728(02)00366-3.

Frankenberg, C., Fisher, J.B., Worden, J., Badgley, G., Saatchi, S.S., Lee, J.E., Toon, G.C., Butz, A., Jung, M., Kuze, A., Yokota, T., 2011. New global observations of the terrestrial carbon cycle from GOSAT: patterns of plant fluorescence with gross primary productivity. Geophys. Res. Lett. 38, L17706. http://dx.doi.org/10.1029/2011GL048738.

Garnier, E., Shipley, B., Roumet, C., Laurent, G., 2001. A standardized protocol for the determination of specific leaf area and leaf dry matter content. Funct. Ecol. 15, 688–695. http://dx.doi.org/10.1046/j.0269-8463.2001.00563.x.

Gausman, H.W., Allen, W.A., Cardenas, R., Richardson, A.J., 1970. Relation of light reflectance to histological and physical evaluations of cotton leaf maturity. Appl. Opt. 9, 545–552. http://dx.doi.org/10.1364/AO.9.000545.

Genty, B., Briantais, J.M., Baker, N.R., 1989. The relationship between the quantum yield of photosynthetic electron transport and quenching of chlorophyll fluorescence. Biochim. Biophys. Acta Gen. Subj. 990, 87–92. http://dx.doi.org/10.1016/S0304-4165(89)80016-9.

Gitelson, A.A., Buschmann, C., Lichtenthaler, H.K., 1998. Leaf chlorophyll fluorescence corrected for re-absorption by means of absorption and reflectance measurements. J. Plant Physiol. 152, 283–296. http://dx.doi.org/10.1016/S0176-1617(98)80143-0.

Gitelson, A.A., Gritz, Y., Merzlyak, M.N., 2003. Relationships between leaf chlorophyll content and spectral reflectance and algorithms for non-destructive chlorophyll assessment in higher plant leaves. J. Plant Physiol. 160, 271–282. http://dx.doi.org/10.1078/0176-1617-00887.

Guanter, L., Frankenberg, C., Dudhia, A., Lewis, P.E., Gómez-Dans, J., Kuze, A., Suto, H., Grainger, R.G., 2012. Retrieval and global assessment of terrestrial chlorophyll fluorescence from GOSAT space measurements. Remote Sens. Environ. 121, 236–251. http://dx.doi.org/10.1016/j.rse.2012.02.006.

Hilker, T., Coops, N.C., Wulder, M.A., Black, T.A., Guy, R.D., 2008. The use of remote sensing in light use efficiency based models of gross primary production: a review of current status and future requirements. Sci. Total Environ. 404, 411–423. http://dx.doi.org/10.1016/j.scitotenv.2007.11.007.

Hogewoning, S.W., Douwstra, P., Trouwborst, G., van Ieperen, W., Harbinson, J., 2010. An artificial solar spectrum substantially alters plant development compared with usual climate room irradiance spectra. J. Exp. Bot. 61, 1267–1276. http://dx.doi.org/10.1093/jxb/erq005.

Jacquemoud, S., Baret, F., 1990. PROSPECT: a model of leaf optical properties spectra. Remote Sens. Environ. 34, 75–91.

Jacquemoud, S., Ustin, S., 2001. Leaf optical properties: a state of the art. 8th International Symposium of Physical Measurements & Signatures in Remote Sensing, pp. 223–332

Jacquemoud, S., Ustin, S., Verdebout, J., Schmuck, G., Andreoli, G., Hosgood, B., 1996. Estimating leaf biochemistry using the PROSPECT leaf optical properties model. Remote Sens. Environ. 56, 194–202. http://dx.doi.org/10.1016/0034-4257(95)00238-3.

Jacquemoud, S., Verhoef, W., Baret, F., Bacour, C., Zarco-Tejada, P.J., Asner, G.P., François, C., Ustin, S.L., 2009. PROSPECT+SAIL models: a review of use for vegetation characterization. Remote Sens. Environ. 113, Suppl, S56–S66. http://dx.doi.org/10.1016/j.rse.2008.01.026.

Joiner, J., Yoshida, Y., Vasilkov, A.P., Middleton, E.M., 2011. First observations of global and seasonal terrestrial chlorophyll fluorescence from space. Biogeosciences 8, 637–651.

Krause, G.H., Weis, E., 1984. Chlorophyll fluorescence as a tool in plant physiology. Photosynth. Res. 5, 139–157. http://dx.doi.org/10.1007/BF00028527.

Kubelka, P., Munk, F., 1931. An article on optics of paint layers. Z. Tech. Phys 12, 593–601.

Lee, J.E., Berry, J.A., Van der Tol, C., Yang, X., Guanter, L., Damm, A., Baker, I., Frankenberg, C., 2015. Simulations of chlorophyll fluorescence incorporated into the Community Land Model version 4. Glob. Chang. Biol. http://dx.doi.org/10.1111/gcb.12948.

Lee, J.E., Frankenberg, C., Van der Tol, C., Berry, J.A., Guanter, L., Boyce, C.K., Fisher, J.B., Morrow, E., Worden, J.R., Asefi, S., Badgley, G., Saatchi, S., 2013. Forest productivity and water stress in Amazonia: observations from GOSAT chlorophyll fluorescence. Proc. R. Soc. B Biol. Sci. 280, http://dx.doi.org/10.1098/rspb.2013.0171.

Lichtenthaler, H.K., Buschmann, C., 2001. Chlorophylls and Carotenoids: Measurement and Characterization by UV-VIS. Current Protocols in Food Analytical Chemistry F4.3.1-F4. pp. 1–8. http://dx.doi.org/10.1002/0471142913.

Meroni, M., Rossini, M., Guanter, L., Alonso, L., Rascher, U., Colombo, R., Moreno, J., 2009. Remote sensing of solar-induced chlorophyll fluorescence: review of methods and applications. Remote Sens. Environ. 113, 2037–2051. http://dx.doi.org/10.1016/j.rse.2009.05.003.

Miller, J.R., Berger, M., Goulas, Y., Jacquemoud, S., Louis, J., Mohammed, G., Moise, N., Moreno, J., Moya, I., Pedrós, R., 2005. Development of a vegetation fluorescence canopy model. ESTEC Contract

Moreno, J., Alonso, L., Delegido, J., Rivera, J., Ruiz-Verdú, A., Sabater, N., Tenjo, C., Verrelst, J., Vicent, J., 2014. Misión FLEX (Fluorescence Explorer): Observación de la fluorescencia por teledetección como nueva técnica de estudio del estado de la vegetación terrestre a escala global. http://dialnet.unirioja.es/servlet/articulo?codigo=4899504&info=resumen&idioma=SPA.

Palombi, L., Cecchi, G., Lognoli, D., Raimondi, V., Toci, G., Agati, G., 2011. A retrieval algorithm to evaluate the Photosystem I and Photosystem II spectral contributions to leaf chlorophyll fluorescence at physiological temperatures. Photosynth. Res. 108, 225–239. http://dx.doi.org/10.1007/s11120-011-9678-5.

Panigada, C., Rossini, M., Meroni, M., Cilia, C., Busetto, L., Amaducci, S., Boschetti, M., Cogliati, S., Picchi, V., Pinto, F., Marchesi, A., Colombo, R., 2014. Fluorescence, PRI and canopy temperature for water stress detection in cereal crops. Int. J. Appl. Earth Obs. Geoinf. 30, 167–178. http://dx.doi.org/10.1016/j.jag.2014.02.002.

Pedrós, R., Goulas, Y., Jacquemoud, S., Louis, J., Moya, I., 2010. FluorMODleaf: a new leaf fluorescence emission model based on the PROSPECT model. Remote Sens. Environ. 114, 155–167. http://dx.doi.org/10.1016/j.rse.2009.08.019.

Porcar-Castell, A., Tyystjärvi, E., Atherton, J., Van Der Tol, C., Flexas, J., Pfündel, E.E., Moreno, J., Frankenberg, C., Berry, J.A., 2014. Linking chlorophyll a fluorescence to photosynthesis for remote sensing applications: mechanisms and challenges. J. Exp. Bot. 65, 4065–4095. http://dx.doi.org/10.1093/jxb/eru191.

Rossini, M., Nedbal, L., Guanter, L., Ač, A., Alonso, L., Burkart, A., Cogliati, S., Colombo, R., Damm, A., Drusch, M., Hanus, J., Janoutova, R., Julitta, T., Kokkalis, P., Moreno, J., Novotny, J., Panigada, C., Pinto, F., Schickling, A., Schüttemeyer, D., Zemek, F., Rascher, U., 2015. Red and far red Sun-induced chlorophyll fluorescence as a measure of plant photosynthesis. Geophys. Res. Lett. 42, 1632–1639. http://dx.doi.org/10.1002/2014GL062943.

Schickling, A., Matveeva, M., Damm, A., Schween, J., Wahner, A., Graf, A., Crewell, S., Rascher, U., 2016. Remotely sensed sun-induced fluorescence significantly improves diurnal modeling of GPP of stressed vegetation. Submit. Remote. Sens. http://dx.doi.org/10.3390/rs70x000x.

W.K., Slaton, M.R., Raymond Hunt, E., Smith, J., 2001. Estimating near-infrared leaf reflectance from leaf structural characteristics. Am. J. Botany 88, 278–284.

Stuckens, J., Somers, B., Delalieux, S., Verstraeten, W., Coppin, P., 2009. The impact of common assumptions on canopy radiative transfer simulations: a case study in citrus orchards. J. Quant. Spectrosc. Radiat. Transf. 110, 1–21. http://dx.doi.org/10.1016/j.jqsrt.2008.09.001.

Tremblay, N., Wang, Z., Cerovic, Z.G., 2011. Sensing crop nitrogen status with fluorescence indicators. A review. Agron. Sustain. Dev. 32, 451–464. http://dx.doi.org/10.1007/s13593-011-0041-1.

Turner, N.C., 1981. Chapter 3: Techniques and experimental approaches for the measurement of plant water status. Plant Soil 58, 339–366. http://dx.doi.org/10.1159/000331745.

Ustin, S.L., Gitelson, A.A., Jacquemoud, S., Schaepman, M., Asner, G.P., Gamon, J.A., Zarco-Tejada, P., 2009. Retrieval of foliar information about plant pigment systems from high resolution spectroscopy. Remote Sens. Environ. 113, S67–S77. http://dx.doi.org/10.1016/j.rse.2008.10.019. Suppl.

Van der Tol, C., Berry, J., Campbell, P., Rascher, U., 2014. Models of fluorescence and photosynthesis for interpreting measurements of solar induced chlorophyll fluorescence. J. Geophys. Res. Biogeosci. 119, 2312–2327.

Van der Tol, C., Verhoef, W., Timmermans, J., Verhoef, A., Su, Z., 2009. An integrated model of soil-canopy spectral radiances, photosynthesis, fluorescence, temperature and energy balance. Biogeosciences 6, 3109–3129. http://dx.doi.org/10.5194/bg-6-3109-2009.

Van Wittenberghe, S., Alonso, L., Verrelst, J., Hermans, I., Delegido, J., Veroustraete, F., Valcke, R., Moreno, J., Samson, R., 2013. Upward and downward solar-induced chlorophyll fluorescence yield indices of four tree species as indicators of traffic pollution in Valencia. Environ. Pollut. 173, 29–37.

Van Wittenberghe, S., Alonso, L., Verrelst, J., Moreno, J., Samson, R., 2015. Bidirectional sun-induced chlorophyll fluorescence emission is influenced by leaf structure and light scattering properties — a bottom-up approach. Remote Sens. Environ. 158, 169–179. http://dx.doi.org/10.1016/j.rse.2014.11.012.

Van Wittenberghe, S., Verrelst, J., Rivera, J.P., Alonso, L., Moreno, J., Samson, R., 2014. Gaussian processes retrieval of leaf parameters from a multi-species reflectance, absorbance and fluorescence dataset. J. Photochem. Photobiol. B 134, 37–48. http://dx.doi.org/10.1016/j.jphotobiol.2014.03.010.

Verhoef, W., 2011. Modelling vegetation fluorescence observations. 7th EARSEL Workshop of the Special Interest Group in Imaging Spectroscopy: Final Programme.

Weis, E., Berry, J.A., 1987. Quantum efficiency of Photosystem II in relation to 'energy'-dependent quenching of chlorophyll fluorescence. Biochim. Biophys. Acta Biomembr. Bioenergetics 894, 198–208. http://dx.doi.org/10.1016/0005-2728(87)90190-3.

Woolley, J.T., 1971. Reflectance and transmittance of light by leaves. Plant Phys. 47, 656–662. http://dx.doi.org/10.1104/pp.47.5.656.

Zhang, Y., Guanter, L., Berry, J.A., Joiner, J., van der Tol, C., Huete, A., Gitelson, A., Voigt, M., Köhler, P., 2014. Estimation of vegetation photosynthetic capacity from space-based measurements of chlorophyll fluorescence for terrestrial biosphere models. Glob. Chang. Biol. 20, 3727–3742. http://dx.doi.org/10.1111/gcb.12664.